Stony Brook University

Effect of support on iron promoted rhodium nanocatalysts for ethanol synthesis from CO hydrogenation

A Thesis Presented

by

Pamela Carolina Carrillo Sanchez

to

The Graduate School

in Partial Fulfillment of the

Requirements

for the Degree of

Master of Science

in

Chemistry

Stony Brook University

August 2015

Stony Brook University

The Graduate School

Pamela Carolina Carrillo Sanchez

We, the thesis committee for the above candidate for the

Master of Science degree, hereby recommend

acceptance of this thesis.

Michael G. White, Thesis Advisor
Professor, Chemistry

Amy C. Marschilok, Chair
Research Associate Professor, Chemistry

Fernando O. Raineri, Third member
Professor, Chemistry

This thesis is accepted by the Graduate School

Charles Taber

Dean of the Graduate School

Abstract of the Thesis

Effect of support on iron promoted rhodium nanocatalysts for ethanol synthesis from CO hydrogenation

by

Pamela Carolina Carrillo Sanchez

Master of Science

in

Chemistry

Stony Brook University

2015

Depleting fossil fuel sources coupled with the deleterious effects of petroleum-based fuel combustion have led to the development of sustainable ways for energy production. One alternative is the production of biofuels like ethanol. Ethanol's biggest advantages are its high energy density, biodegradability and carbon neutrality. A potential scalable process is the conversion of synthetic gas (syngas: CO, CO_2, H_2) produced from gasification of biomass with the use of Rh-based catalysts. The work presented in this thesis aimed to study the effect of the introduction of 1, 5, and 10 wt % CeO_2 into a TiO_2 support on Fe promoted-Rh catalysts for ethanol production from CO hydrogenation. The mixed-oxide CeO2-TiO2 support was synthesized by a sol-gel method where Rh and Fe nanoparticles were deposited by wet incipient impregnation. Reactivity studies were carried under CO hydrogenation conditions with the use of gas chromatography. Characterization of the bare support and the catalyst that showed the best ethanol selectivity were performed by in-situ X-ray diffraction synchrotron experiments. Ethanol selectivity increases with ceria content with a shift on product distribution and CO conversion rates compared to Rh supported on single TiO_2 and CeO_2. This could be explained by a

synergetic effect between CeO_2 and TiO_2 and to the to the formation of amorphous and mobile species of CeO_x that can act as dispersing agents for the Rh particles increasing catalytic sites for CO insertion and for the stabilization of HCO_x species. XRD characterization analysis of 10%CeO_2-90%TiO_2 identified three crystallographic phases: anatase, TiO_2(B), and cerianite. The unpromoted 2%Rh/10%CeO2-90%TiO2 in-situ XRD analysis showed an absence of Rh^0 under CO hydrogenation conditions. Conversely, the addition of Fe to the different mixed-oxide compositions showed comparable ethanol selectivity at the expense of methane formation. Therefore, the introduction of ceria into the titania support on unpromoted Rh-based catalysts affects ethanol selectivity largely while when doped with Fe such effect is suppressed.

Dedication Page

Para Pulgos, Yolita, y Reina

Table of Contents

List of Figures

List of Tables

List of Abbreviations

Syngas: Synthetic Gas

WGS: Water Gas Shift

RWGS: Reverse Water Gas Shift

FTS: Fischer–Tropsch Synthesis

DFT: Density Functional Theory

NP: Nanoparticles

RLS: Rate Limiting Step

SCS: Selectivity Controlling Step

GHSV: Gas hourly space velocity

STM: Scanning Tunneling Microscope

Acknowledgments

First of all, I would like to thank my parents who have always supported me and showed their love regardless of the distance. Another very important person, my aunt, Yolanda, has been a key family member in my upbringing and has made possible for me to pursue my graduate studies. Also, I want to thank my brothers and their families for all for their kind, caring, and supportive words.

I want to greatly thank my thesis advisor Prof. Michael White who has been an exceptional mentor who has guided me through the whole process and has made this work possible. I feel very fortunate to be part of such cooperative and fun research group as is White's group. Particularly, I deeply appreciate the help and supervision of Robert Palomino. I would like to acknowledge the aid offered by Prof. Peter Khalifah and Diane Collabelo and their insightful discussions regarding the XRD data analysis.

I have been able to pursue my M.Sc. studies with the financial help of the Fulbright Foreign Program, Senescyt Grantee Program, and Delta Kappa Gamma Worldwide Fellowship. I would also like to mention some other important people that have offered me their unconditional friendship and support, my friends from Ecuador: Miaus, Dani, Cris, Erika and Pauli, and my friends from graduate school in Stony Brook University, specially, Cee, Ramiro, Alejandro, and Paul.

The experiments were carried out in the Chemistry Department at Brookhaven National Laboratory under Contract No. DE-AC02-98CH10086 with the U.S. Department of Energy (Division of Chemical Sciences, Geoscience and Biosciences). XRD experiments were possible with the funding provided by the Joint Photon Science and approval of Prof. John Parise. I am thankful for the support provided by the beamline scientists of 11-ID-B at APS Dr. Kevin Beyer and Dr. Karena Chapman.

CHAPTER 1

1. INTRODUCTION

The ever-increasing global energy consumption has caused a high demand on petroleum-based fuels. As of 2012, 41% of the energy consumed worldwide was oil-based, 64% of which corresponds to the transportation sector alone (Figure 1).[1] Oil-based fuels cause a detrimental environmental impact mainly because of their greenhouse gases emissions. The ever-dwindling supply of crude oil for producing transportation fuels also impacts availability and crude oil price.[2] Although there are potentially many alternative sources for electricity, e.g., solar, wind and nuclear, the slow progress of high capacity storage batteries has generated a need for the development of alternative and sustainable sources of liquid fuels suitable for transportation vehicles. Biofuels are very attractive since they can be derived from common biomass sources, are carbon neutral, biodegradable and cost-wise competitive compared to traditional fuel sources.[3] Ethanol is currently the most widely produced bio-derived liquid fuel. The U.S. ethanol primarily as gasoline additive whereas other countries like Brazil uses it as fuel. Ethanol's advantages are its compatibility with the existing infrastructure, high energy density, high octane number, cleaner emissions and that it can be produced from renewable feedstocks.[4] Although ethanol has been primarily produced through biochemical routes, thermochemical processes like conversion of synthetic gas (syngas: CO, CO_2, H_2, and H_2O) produced from biomass gasification are of high interest since they can potentially be scalable.

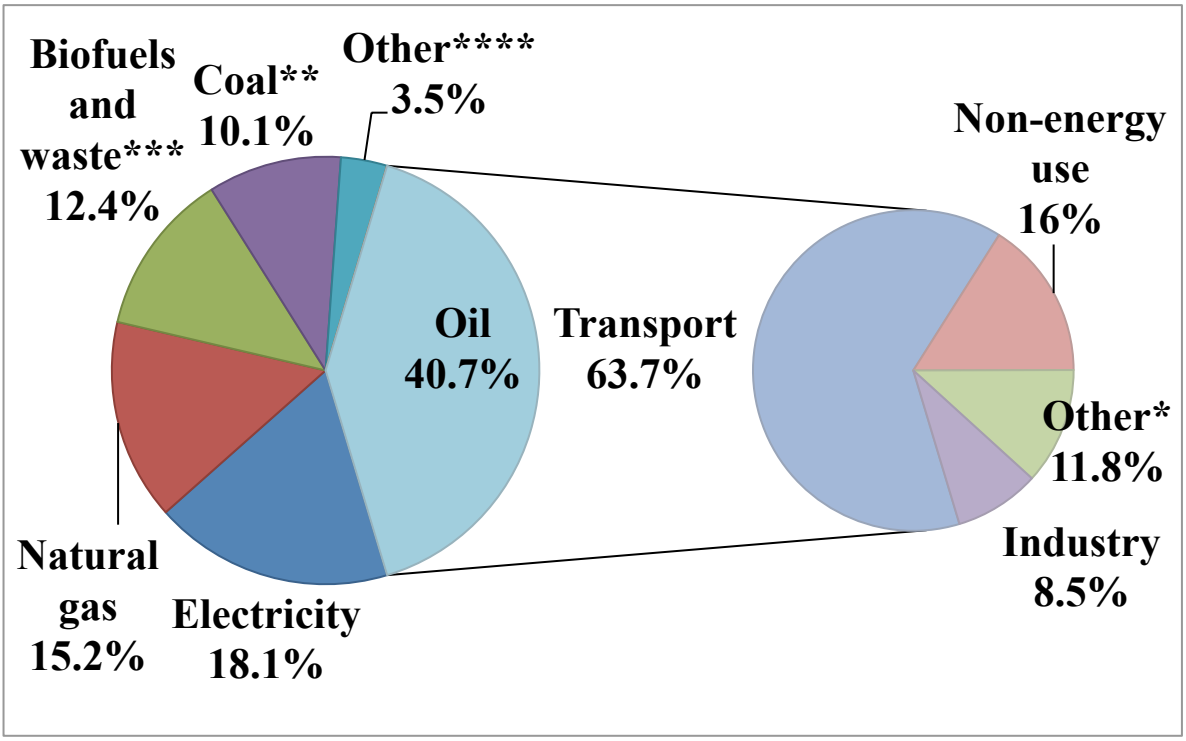

Figure 1. Energy consumption distribution: 2012 fuel shares of total final consumption and 2012 shares of world oil consumption. *Includes agriculture, commercial and public services, residential, and non-specified other. **In these graphs, peat and oil shale are aggregated with coal. ***Data for biofuels and waste final consumption have been estimated for a number of countries. ****Includes geothermal, solar, wind, heat, etc. Adapted from reference [1].

1.A Reactions involved in ethanol synthesis from syngas conversion

Direct synthesis of ethanol from syngas involves several reaction pathways that produce a variety of products that are altered by kinetic and thermodynamic constraints. Thus, it is important to describe the individual reactions that are involved in ethanol production from the components of syngas: CO, CO_2, H_2 and H_2O. The overall reaction of ethanol synthesis involves hydrogenation of CO (Reaction 1) and CO_2 (Reaction 2).[5,6]

$$2CO + 4H_2 \rightarrow C_2H_5OH + H_2O \quad (1)$$

$$\Delta H^o = -257.04\ kJ\ mol^{-1}$$

$$\Delta G^o = -123.14\ kJ\ mol^{-1}$$

$$2CO_2 + 6H_2 \rightarrow C_2H_5OH + 3H_2O \quad (2)$$

$$\Delta H^o = -174.42\ kJ\ mol^{-1}$$

$$\Delta G^o = -65.94\ kJ\ mol^{-1}$$

Under standard reactions conditions, both hydrogenation reactions are exothermic and thermodynamically favorable. The effects of temperature (0 to 1000 °C) on the gas-phase equilibrium compositions for reactions (1) and (2) calculated based on $\Delta G_r^o = -RTlnK_{eq}$ are shown in Figure 2 for CO/CO_2 hydrogenation.[5]

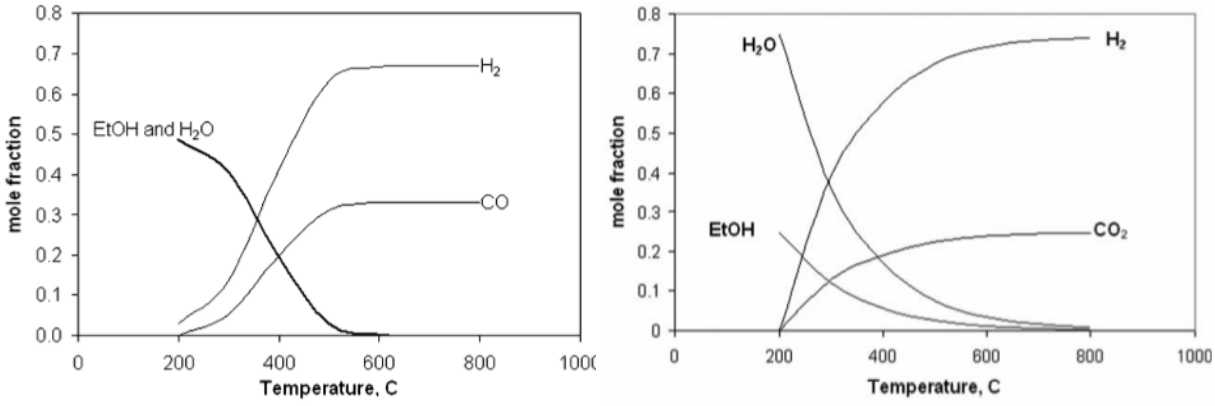

Figure 2. Equilibrium composition for the hydrogenation of CO (a) and CO2 (b) to ethanol at 2:1 H_2:CO2 and 3:1 H_2:CO, respectively, at 30 bar (calculated using AspenPlus®). From reference [5].

The reactions that affect CO and CO_2 hydrogenation the most are methanation (Reaction 3) and the water-gas-shift reaction (Reaction 4).[6]

$$CO \quad + 3H_2 \rightarrow CH_4 + H_2O \tag{3}$$

$$\Delta H^o = -205.9 kJ\ mol^{-1}$$

$$\Delta G^o = -141.9\ kJ\ mol^{-1}$$

Methane production consumes a significant amount of H_2 and methane is the thermodynamically preferred product over at all temperature compared to ethanol formation (Figure 3). To favor the direct conversion of CO to ethanol temperatures below 280°C are needed (Figure 2 (a)).[6]

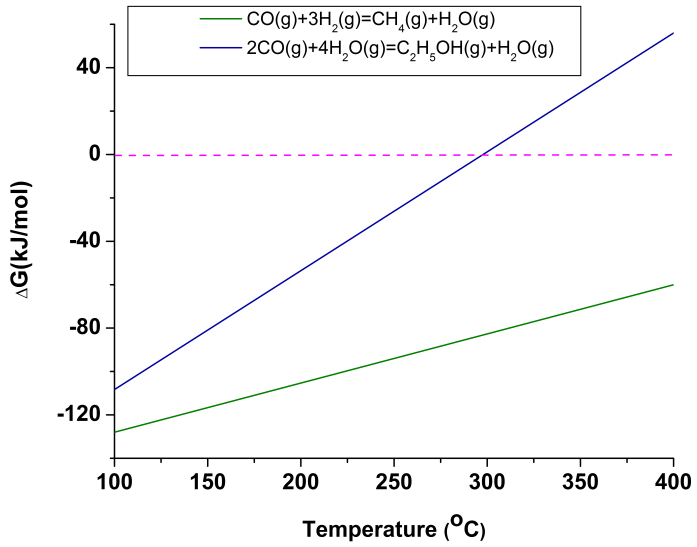

Figure 3. Free-energy changes in the hydrogenation of CO to ethanol (blue) and methane (green). Adapted from reference [6].

The water gas shift reaction (WGS) alters the equilibrium of both CO and CO_2 hydrogenation. Ethanol produced by CO hydrogenation produces water that reacts with CO to produce CO_2 and hydrogen, i.e., (Reaction 4).

$$H_2O + CO \leftrightarrow CO_2 + H_2 \quad (4)$$

$$\Delta H^o = -41.1\ kJ\ mol^{-1}$$

$$\Delta G^o = -28.6\ kJ\ mol^{-1}$$

Conversely, the reverse WGS (RWGS) affects CO_2 hydrogenation by producing CO. [5,7] At elevated temperatures, the WGS reaction is not thermodynamically favorable. This is illustrated by the decline and sign change in ΔG as a function of temperature.[8]

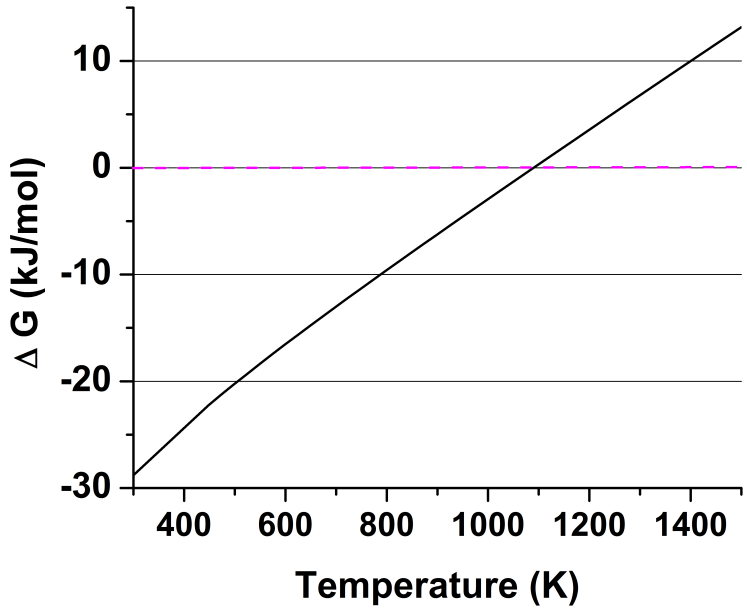

Figure 4. Thermodynamic equilibrium of the WGS reaction as described by the Gibbs free energy change as function of temperature. Adapted from reference [8].

As it has been described, the direct formation of ethanol by CO hydrogenation is a complex reaction pathway that is affected by two side reactions: methanation and the WGS reaction. Methane formation needs to be suppressed since it is more thermodynamically stable than ethanol. The WGS affects the equilibrium of the reaction due to CO

consumption and H_2 production. Therefore, in order to overcome thermodynamics and kinetic energetic barriers for achieving high ethanol yields, low temperature, optimal $CO:H_2$ gas feeds, and the use of catalysts are required.

1.B HETEROGENEOUS CATALYSTS FOR CO/CO_2 HYDROGENATION

Syngas transformation to ethanol can be directly achieved by heterogeneous catalysis using metal-based catalysts. As we have previously discussed, hydrogenation of CO and CO_2 for ethanol production is a challenging process due its slow kinetics and low selectivity. Studies using realistic syngas composition are limited. Most studies are focused on CO hydrogenation, and in minor proportion on hydrogenation of CO_2 and mixtures of CO and CO_2. This is mainly due to the fact that alcohols can be produced from syngas through RWGS, which converts CO_2 to CO, followed by CO-hydrogenation that leads to alcohol formation.[9,10] Four main types of catalysts have been investigated: modified methanol synthesis (based on Cu), modified Fischer–Tropsch, modified Mo-based catalysts, and Rh based catalysts.[5,6] The first three types are discussed briefly and some examples are illustrated in Table 1 to compare their activity and carbon selectivity towards ethanol. Then, Rh-based are described more in detail.

Table 1. Catalyst Used in the Direct Conversion of Syngas to Ethanol and Mixed Alcohols

Catalyst	Experimental conditions				Carbon selectivity (%)			
	Temp (^{O}C)	Press (psig)	H_2/ CO	CO conversion (%)	Hydrocarbons	Methanol	Ethanol	C_{3+} alcohols
Modified high-temperature Cu–free ZnO/Cr_2O_3								
3 mol% $Cs/ZnO/Cr_2O_3$[11]	405	110	0.75	4.5	6.5	24	<1.0	69
1% $K/ZnO/Cr_2O_3$[12]	400	1500	1	19	NA	34	0	66
Modified low-temperature Cu/ZnO methanol catalysts								
0.8 mol% $Cs/Cu/Zn/Cr_2O_3$[13]	310	1100	0.45	21	14	NA	30[a]	
0.3 mol% $Cs/Cu/Zn/Al_2O_3$[13]	310	1100	0.45	14	6.5	NA	10[a]	
Modified Fisher-Tropsch								
Co-Re-Sr/SiO_2[14]	250	300	2	4.9	63	4.7	22	N/A
Fe/Al_2O_3[15]	200	116	2	<1.0	42	20	3.0	N/A
Co-Ir-Sr/SiO_2[16]	220	305	2	2.2	34	8.7	37	N/A
Modified Unsulfided Mo-based								
1%K-Co_1Mo_4[17]	300	870	2	24	60	21	13	8.4
K-Ni-β-Mo_2C (K/Mo=0.2)[18]	300	1160	1	73	26	6.0	9.4	7.2
K-Co-β-Mo_2C (Mo/Co=10)[19]	300	1160	1	37	61	11	14	24
Modified Sulfided Mo-based								
MoS_2 (Dow Chemical)[20]	295	1050	1	29	14	23	41	17
$KCoMoS_2$/ C (Mo/Co=16)[21]	330	725	2	8.7	61	20	16	5.6
$CsCO_3CoMo_2$/clay[22]	320	2000	1	29	31	11	30	22

[a] Carbon selectivity includes ethanol and C_3^+ alcohols

Most of the studies discussed below are based on the use of oxide supported Rh nanocatalysts since they offer advantages over their bulk counterparts like higher surface area, control of their compositions, sizes, and surface morphologies that offers catalytic

active sites that can trigger heterogeneous processes.[23] The catalytic activity of nanocatalysts is governed by particle size, oxidation state, and chemical/physical environment[24]. Thus, it is important to understand the relationship between these factors, and catalyst reactivity and selectivity in order to design a highly efficient ethanol nanocatalyst. These can be modified by the addition of a metal promoter or support that can suppress methane formation with the enhancement of C-C formation.[25]

1.B.1 Modified methanol Synthesis Catalysts

Two types of modified-methanol synthesis catalysts are widely used: high-temperature Cu –free ZnO/Cr_2O_3, and low-temperature Cu/ZnO methanol catalysts.[6,26] The side production of higher alcohols and ethanol was observed when methanol synthesis was performed using these catalysts, which was improved when alkali metals remained as impurities.[27] High temperature methanol catalysts work at 350-450 °C and 120-300 atm (1700-4410 psig) that produce methanol as main product and small quantities of ethanol.[28,29, 30] Alkali promoters (Li, Na, K,Cs) need high temperatures, which still remains a problem as it leads to large yields of hydrocarbons.[12,31,32] Thus, the most studied catalysts are Cu-based, i.e., Cu nanoparticles supported on a metal oxide powder such as ZnO. These work in a temperature range between 275 °C and 310 °C and pressure range between 750 and 1500 psig.[28,29,30] Common supports are ZnO, Al_2O_3 or Cr_2O_3 that when impregnated with an alkali produce short linear and branched alcohols, and small amounts of hydrocarbons and oxygenates.[27,33,34,35] Alkali promoters that enhance alcohol selectivity follow the trend: Cs>Rb>K>Na>Li.[26]

1.B.2 Modified Fischer-Tropsch Catalysts

Fischer–Tropsch (FT) synthesis catalysts are commonly used for the production of long chain hydrocarbons and can form small yields of oxygenates, including ethanol.[36] These are typically composed of Co, Ru, Fe or Ni metals supported on SiO_2 or

Al_2O_3.[37,15,38,39,14] The selectivity and yield of oxygenates produced can be enhanced by adding other transition metal and alkali cations. Transition metal promoters (Cu, Mo, Mn, Re, Ru), and alkali (Li, K, Cs, Sr) promoters have been widely used. The design of such catalysts depends on the nature and loading of the promoter, type of alkali, and support, all of which govern alcohol selectivity and yield.[39,14,35,34]

1.B.3 METAL SULFIDE CATALYSTS

Two major types of Mo-based catalysts are known: sulfided and unsulfied. Unsulfided Mo- based catalysts are promoted by adding base, alkali, and noble metals. Alkali metals increase alcohol selectivity compared to hydrocarbons for CO hydrogenation.[40] Some examples are K-promoted Mo supported on activated carbon that show 10-15% ethanol selectivity,[17] and K-promoted Co or Ni-doped β-Mo_2C.[18,19] As for the sulfide Mo-based catalysts, a basic promoter metal is preferred. Ethanol selectivity increases in the order: Li, Na, Cs, Rb , K.[41] Schulz–Flory distribution rules selectivity to alcohols on alkali promoted Mo catalysts and limits higher alcohol formation. On the other hand, improved C_2^+ alcohol selectivity is achieved with transition metals like Co, Mn or Ni.[42,43, 43]

1.B.4 RH-BASED CATALYSTS

Rh-based catalysts are the most studied and best performing systems due to their ethanol selectivity in CO hydrogenation. These are preferred because of their low working temperatures (150-350^{O}C) and pressures (14.5-360 psi).[44] It has been widely known that supported Rh has the ability to produce C_2^+ oxygenates like ethanol, acetaldehyde and acetic acid selectively from syngas. Rhodium has the advantage of being located between metals (Fe, Co) that easily dissociate CO to form hydrocarbons and metals (Pd, Pt and Ir) that do not dissociate CO and thereby produce ethanol.[5]

There is no consensus on the mechanism of CO hydrogenation with the use of Rh-based catalysts. The majority of studies suggest CO dissociation and insertion is initiated by H_2 and CO adsorption. The CO molecules that do not dissociate undergo hydrogenation to form methanol or surface hydrocarbon species $(CH_x)_{ad}$. The hydrocarbon species produce methane or higher hydrocarbons by hydrogenation or C_2 oxygenates by CO insertion. The C_2 oxygenates are able to undergo hydrogenation to form ethanol.[45,46,47,48,49]

To further understand the CO hydrogenation reaction pathway, density function theory calculations were performed by Choi and Liu on a Rh(111) surface (see Figure 4).[25] It was determined that the reaction starts with CO hydrogenation to form formyl (HCO), which is the rate-limiting step. Three major products were identified, CH_4, CH_3OH and C_2H_5OH, and the selectivity to ethanol is controlled by CH_4 formation, CO insertion and C-C formation. One of the major obstacles for obtaining high ethanol selectivity is the strong Rh-CO interaction, which can poison the surface and produce high yields of methane.

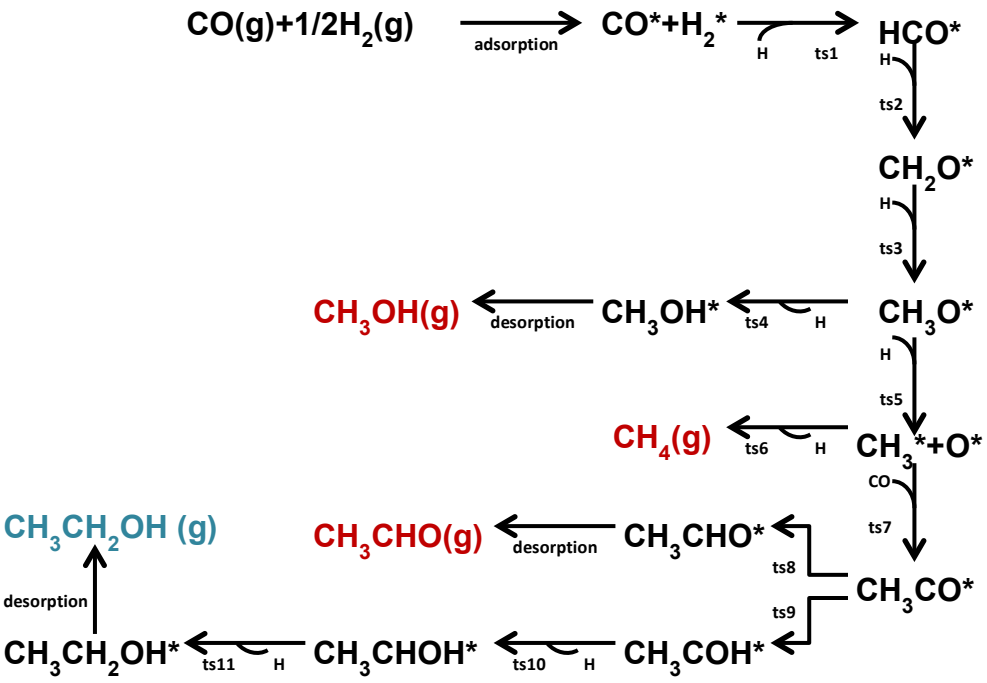

Figure 5. Scheme of the reaction pathway for ethanol synthesis from CO and H_2 on Rh (111). Adapted from reference [25].

The performance of Rh-based catalysts can be improved when metal promoters are added that aid CO dissociation and CO insertion while suppressing hydrogenation of $(CH_x)_{ad}$ intermediates.[45] Transition metals like Mn, Ti, and Zr have been found to increase CO conversion and C_2 oxygenate selectivity when added to Rh/SiO_2 catalysts. Others metals like Fe and Mo on Rh/ZrO_2 catalysts improve chain growth and formation of C_2^+ compounds.[44] Ethanol selectivity enhancement has been also reported when lanthanides, vanadium, silver, and cerium have been added to supported rhodium-based catalysts.[5]

Recently, DFT studies were performed in order to understand the role of Fe, Mo, and Mn doping of Rh(111) surfaces for ethanol synthesis from CO hydrogenation. The theoretical studies were constrained to the rate limiting step (rls) (formyl formation) and selectivity-controlling step (scs) (CH_4 formation) due to the complexity of the CO hydrogenation reaction. Promoter type and its position on the surface or subsurface layer of the catalyst was found to play a determining role in ethanol selectivity and overall reactivity. Fe prefers to stay on the surface and produces the largest ethanol selectivity. Conversely, Mo showed the highest overall yield and reactivity and was found to be located at the surface layer[50].

One of the best metal promoters of Rh-based catalysts is Fe which results in an increase in ethanol selectivity with increasing Fe loading.[51] The highest ethanol selectivity was achieved with a 10% wt. Fe loading for Rh/Al_2O_3, which was attributed to the decrease of methane selectivity and enhancement of CO insertion. The effect of Fe loading has also been tested for Rh-based catalysts supported on silica and titania.[52] The addition of 1 wt% Fe to 2 wt% Rh/SiO_2 showed a 22% selectivity to ethanol, and methane as primary side-product, while, 1 wt% Fe-2 wt% Rh/TiO_2 improved CO conversion, and oxygenate selectivity. Moreover, maximum ethanol selectivity (37%) was achieved for a Fe loading of 5% wt on Rh/TiO_2.

1.B.4.A Influence of catalyst support

The design of efficient Rh-based catalysts for ethanol production from CO hydrogenation can also be influenced by the choice of oxide support. The choice of oxide support can have a significant effect on ethanol selectivity by modifying the grade of Rh dispersion and how CO is adsorbed (dissociately or non- dissociately).[5] It has been found that ethanol selectivity decreases in the order: Rh/La_2O_3> Rh/TiO_2> Rh/SiO_2> Rh/Al_2O_3.[53] Another transition metal oxide that was been tested for its ethanol selectivity has been cerium dioxide.[54] The use of 2 wt% Rh/CeO_2 produces more than double of C_2^+ oxygenate selectivity than 2 wt% Rh/ SiO_2 caused by hydrocarbon suppressed formation. The main oxygenate product formed by Rh/CeO_2 is ethanol while Rh/SiO_2 produces mainly acetaldehyde and only traces of ethanol. The effects of different supports have been attributed to their electron withdrawing/donating capability which influences reducibility of the metal and the morphology of the metal NP.[55]

The effects of SiO_2, TiO_2, and the mixed oxide SiO_2-TiO_2 as supports for Rh-based catalysts have also been investigated using Mn and Li as promoters.[56] The mixed oxide exhibited an improved catalytic performance for CO conversion, and C_2^+ oxygenates and ethanol selectivity compared to the use of single oxide supports. Moreover, SiO_2 has been compared to ZrO_2 and to SiO_2 -ZrO_2 mixed oxides with various molar ratios as supports promoted by the addition of Mn and Li.[57] The study showed that the mixed oxide support has a significant effect on catalytic activity and selectivity which depends on the ratio of Si:Zr in the mixed oxide. The highest ethanol selectivity and activity was achieved with the mixed oxide with a Si:Ti ratio of 1:3.

Mixed oxides are now raising interest for several heterogeneous catalytic processes due to their unique structural and electronic properties compared to the single oxide counterparts.[58] These properties can be explained by the introduction of stress into the lattice of the oxides or to atypical coordination modes. This produces diverse metal-metal, metal-oxygen, metal-mixed-oxide interactions that finally lead to electronic states not seen in single-metal oxides supports. The CeO_x-TiO_2 mixed-oxide has drawn a particular

attention in catalytic processes due its ability to catalyze processes like CO oxidation and the WGS reaction. For example, the mixed oxide support in the Au/CeO_x-$TiO_2(110)$ system greatly improved the CO oxidation activity compared to $Au/TiO_2(110)$, $CeO_x/Au(111)$, $Au/CeO_2(111)$, Cu/ZnO(0001), and copper single crystals.[59,60]

CeO_2 and TiO_2 have been used as supports for promoted Rh-based catalyst for ethanol production from CO hydrogenation but their CeO_2-TiO_2 mixed-oxide has not been studied for this reaction. To our knowledge there is only one study that investigated the effect of the ceria as a promoter for CO hydrogenation rather than as support.[61]The reaction pathway of CO hydrogenation shares elementary reaction steps with the WGS reaction such as the formation of HCO_x species.[62,63] The presence of Ce^{+3} stabilizes HCO_x species without the aid of an admetal,[58,64] which has been identified as the rls in CO hydrogenation on Rh-based catalysts, i.e., the formation of HCO.[25] The properties exhibited by CeO_2-TiO_2 mixed-oxides alone provides them to be support candidates that can enhance ethanol synthesis from CO hydrogenation, which can be further improved by the addition of active metals on their surfaces.

1.C STUDIES PERFORMED IN THIS THESIS

Due to the complexity of the CO hydrogenation reaction, a multicomponent catalyst that provides diverse active sites for the several reactions steps can provide enhanced reactivity and ethanol selectivity. Mixed oxides can offer this type of advantage due to the presence of various metal-metal, metal-oxide, and metal-promoter interactions that are translated in unique morphological, electronic and structural properties. The CeO_2-TiO_2 system has been used to improve catalytic processes similar to CO hydrogenation, and shown the ability to stabilize formyl species (rls in CO hydrogenation in Rh-based catalysts). Thus, it is expected that this mixed oxide support can improve ethanol selectivity in Rh-based nanocatalysts.

The work presented in this thesis aimed to investigate the effect of a mixed-oxide

CeO_2/TiO_2 as support on Fe-promoted Rh-based catalysts for ethanol production from CO hydrogenation. The mixed-oxide support was synthesized by a sol-gel method followed by the addition of FeRh alloy nanoparticles by wet incipient impregnation. Reactivity studies were carried under CO hydrogenation conditions with the use of gas chromatography to establish the product distribution from which activity and selectivity could be derived. Finally, the bare support and the catalyst that showed the best ethanol selectivity were structurally characterized by in-situ x-ray diffraction synchrotron experiments performed at 11-ID-B in APS at Argonne National Laboratories.

CHAPTER 2

2. EXPERIMENTAL

2.A. SYNTHESIS OF SAMPLES

Mixed oxide supports of CeO_2-TiO_2 were synthetized by a modified[65] sol-gel technique described by Fang[66] and Gionco[67]. The process is represented in pictures in Figure 6. For this, 10 g titanium (IV) butoxide (Aldrich®, reagent grade 97%) was weighed. Then, 3 ml of glacial acetic acid (CH_3COOH) and 40 ml of absolute ethanol (C_2H_5OH) were added and mixed under stirring to form Solution A. The pH of A was adjusted between 2.3-2.7 with a calibrated pH meter with hydrochloric acid. Solution B was prepared by dissolving stoichiometric amounts of cerium (III) nitrate hexahydrate (Aldrich ® 99% trace metal basis) with 3 ml of distilled water and 20 ml of absolute ethanol. Solution B was added to A under stirring in a drop-wise fashion until the formation of a stable sol. The sol was aged in air until a gel was produced. The gel was dried at $75^{O}C$ for 72 h, calcined at $450^{O}C$ for 2 h, and grinded with a mortar and pestle. For the single supports, cerium (III) nitrate hexahydrate (Aldrich ® 99% trace metal basis) and titanium (IV) isopropoxide (Aldrich®, reagent grade 99%) were used as precursors for the synthesis of CeO_2 and TiO_2, respectively, following the previously method described. The concentrations of the three mixed oxides prepared by the described procedure were 1, 5 and 10 wt % CeO_2, these will be hereafter labeled as 1CeTi, 5CeTi and 10CeTi, respectively.

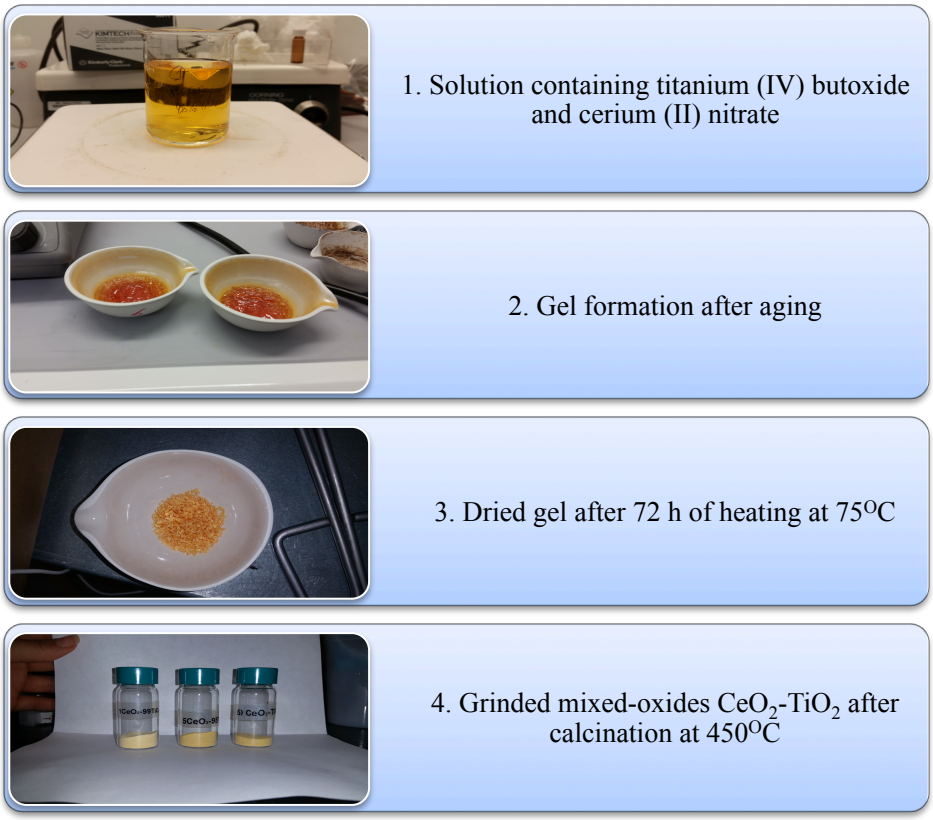

Figure 6. Graphic evolution of the sol-gel synthesis of CeO_2-TiO_2 mixed-oxides

The samples prepared are detailed in Table 2 with its respective composition (determined by weight) and labels. Stoichiometric amounts of rhodium nitrate hydrate (Aldrich®) and iron (III) nitrate nonahydrate (Aldrich®, ≥99% trace metal basis) were weighed and dissolved in 1 ml of distilled water. The solution was added in a drop-wise manner to the mixed oxide powder support until a paste was formed. The paste was dried overnight at 240 ^{O}C, calcined in air at 450 ^{O}C for 4h, and grinded until a powder was obtained.

Table 2. Synthetized Fe-modified Rh/CeO2-TiO2 catalysts samples								
Label	**Rh wt (%)**	**Fe wt (%)**	**Label**	**Rh wt (%)**	**Fe wt (%)**	**Label**	**Rh wt (%)**	**Fe wt (%)**
2Rh/1CeTi	2.0	-	**2Rh/5CeTi**	2.0	-	**2Rh/10CeTi**	2.1	-
2.5Fe/1CeTi	-	2.5	**2.5Fe/5CeTi**	-	8.0	**3Fe/10CeTi**	-	2.9
1Fe2Rh/1CeTi	2.0	1.0	**1Fe2Rh/5CeTi**	2.0	1.0	**1Fe2Rh/10CeTi**	2.0	1.0
2.5Fe2Rh/1CeTi	2.0	2.5	**2.5Fe2Rh/5CeTi**	2.0	2.5	**4Fe2Rh/10CeTi**	2.2	3.5
5Fe2Rh/1CeTi	2.0	5.0	**5Fe2Rh/5CeTi**	2.0	5.0	**5Fe2Rh/10CeTi**	1.9	5.0
8Fe2Rh/1CeTi	2.0	8.0	**8Fe2Rh/5CeTi**	2.0	8.0	**8Fe2Rh/10CeTi**	1.8	8.0

2.B. REACTIVITY STUDIES

In order to determine the carbon selectivity of CO hydrogenation to molecular compounds, reactivity studies were performed. The synthetized catalysts were evaluated in a flow-cell reactor illustrated in Figure 7(a).[68] The weighed catalyst (40 mg) was loaded into a 1/8" OD glass capillaries using glass wool as plugs. Heating was delivered to the sample by a filament around the capillary connected to a power supply. Temperature was monitored with a thermocouple inserted inside the quartz capillary with the loaded sample, and connected to a digital temperature reader. The gases, CO and H_2, used were UHP grade and controlled by mass flow controller (MKS instruments). First, 9 ml/min of H_2 at 1 bar (gas hourly space velocity (GHSV)= 0.028 $mL \cdot min^{-1} \cdot mm^{-3}$) was flowed for 10 min, and then the sample was reduced for 30 min at $300^{O}C$. Then, the gas flow was changed to CO and H_2 to 2 ml/min and 4 ml/min at a pressure of 1 bar (GHSV=0.019 mL/min mm^3), respectively, for 10 min, and temperature was raised to $240^{O}C$. This temperature has shown the best activity and selectivity for oxygenate and ethanol production for CO hydrogenation.[69]

The downstream of reactants and products were analyzed by a gas chromatograph (an Agilent © 3000 Micro GC), connected to the output of the reactor via heated 1/8" OD stainless steel tube, until the steady state was reached, approximately 2 h. The gas chromatograph is equipped with three micro columns separated in channels, and a TCD

detector. Channel A correspond to MS-5A PLOT column used to detect carbon monoxide and methane. Channel B has a Agilent PLOT-U column that was used to detect higher hydrocarbons. Finally, Channel C equipped with a Stabilwax column for the identification of oxygenate compounds present in the gaseous stream. The product concentration was determined by calibration curves for each compound, and CO conversion and product selectivity were calculated using Equations 5 and 6, respectively

$$\%\ CO\ Conversion = \sum \frac{n_i \cdot M_i}{M_{CO}} \cdot 100\% \quad (5)$$

where n_i is the number of carbon atoms in product i, Mi is the percentage of product i detected, and M_{CO} is the percentage of carbon monoxide in the gas feed. On the other hand, the selectivity is based on the total number of carbon atoms and is defined in Equation 6 where Si is the selectivity to product i.

$$S_i = \frac{n_i \cdot M_i}{\sum n_i \cdot M_i} \cdot 100\% \quad (6)$$

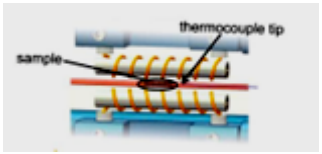

(a)

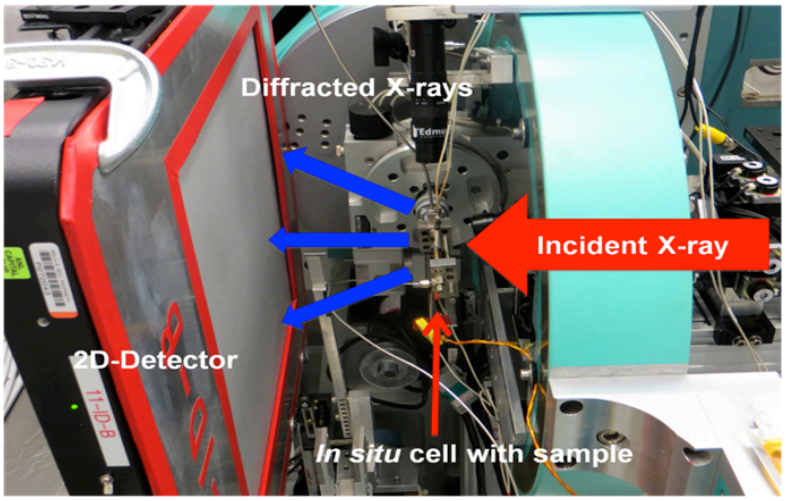

(b)

Figure 7. (a) Flow-cell/furnace and relative position of the sample and thermocouple tip within the furnace hot zone. Taken from reference [68]. (b) Experimental setting for in-situ XRD synchrotron experiments.

2.C CHARACTERIZATION BY IN-SITU XRD

XRD measurements were performed at the 11-ID-B beamline at the Advance Photon Source in Argonne National Laboratory (Figure 7(b)). The operating energy was 55.6 keV using the Si(311) monochromator that provided a wavelength of 0.2114 Å. A Perkin Elmer amorphous silicon 2-D detector was used at a distance from the sample of 900 mm. Calibration was performed using a cerium dioxide standard. X-ray diffraction measurements were performed using the same flow-furnace reactor with the use of 1.2-mm OD quartz capillaries and quartz wool, and settings as the reactivity measurements. Data was collected for the samples for the as-synthetized, reduced and under CO hydrogenation reaction conditions. XRD data was also collected for the synthetized bare support of 10%CeO_2-90%TiO_2, titania and ceria to characterize their structure.

The XRD diffraction images were converted into 1-D 2-theta scans using the Fit2D[70] software. Rietveld refinement was performed with the use of EXPGUI-GSAS[71,72] software. The fitting of the samples we done using models where lattice constants, scale factors, and peak profile functions were used to achieve a simulated diffracting pattern almost identical to the collected data. The models were elected based on previous studies and on knowledge of synthesis and reaction conditions. A complete fitting provided with information about phase quantification and lattice parameter determination.[69]

CHAPTER 3

3. RESULTS AND DISCUSSION

3.A REACTIVITY AND SELECTIVITY STUDIES

3.A.1 RH-ONLY CATALYSTS

Table 3 shows the CO conversion and carbon selectivities of several Rh-catalysts supported on ceria-modified titania, and single supports of CeO_2 and TiO_2. For purposes of comparison, the values have been also plotted in Figure 8 and 9. The bare supports and samples containg only iron as admetal were also tested. The mixed-oxide showed no activity while the Fe/CeTi samples show just the formation of ethane traces.

Table 3. CO conversion and selectivity of unpromoted Rh catalysts

Support (wt %)	Conditions	CO Conv. (%)	Selectivity (%)				
			CH_4	C_2^+ hydrocarbons	CH_3OH	CH_3CH_2OH	C_2^+ oxygenates
2%Rh/10%CeO_2-90%TiO_2	1 bar, 513K, H_2:CO=2	2.1	57	20	2.2	18	2.7
2%Rh/5%CeO_2-95%TiO_2	1 bar, 513K, H_2:CO=2	3.3	62	20	1.7	14	2.8
2%Rh/1%CeO_2-99%TiO_2	1 bar, 513K, H_2:CO=2	4.7	51	35	1.2	9.3	3.4
1%Rh-10%CeO_2/TiO_2[61]	30 bar, 573K, H_2:CO=2	9.2	65	3.8	5.5	16	3.3
1%Rh-5%CeO_2/TiO_2[61]	30 bar, 573K, H_2:CO=2	12	64	3.7	5.5	15	3.5
1%Rh-1%CeO_2/TiO_2[61]	30 bar, 573K, H_2:CO=2	32	47	2.2	11	33	4.7
2%Rh/CeO_2 [a]	1 bar, 513K, H_2:CO=2	0.85	47	19	3.1	28	2.5
1% Rh/CeO_2 [a]	1 bar, 513K, H_2:CO=1	0.54	35	--	--	59	6.0
2%Rh/TiO_2[69]	1 bar, 513K, H_2:CO=2	11	60	33	0.4	3.7	3.4
2% Rh/TiO_2[52]	20 bar, 543K, H_2:CO=1	5.7	47	23	1.9	11	16

[a] **Measurements performed in our laboratory.**

The 2% wt. Rh on the ceria modified titania catalysts show a higher catalytic activity towards ethanol production in comparison to Rh supported on TiO_2 but with lower CO conversion under the same reaction conditions (Table 3). The enhanced alcohol selectivity can be attributed to C_2^+ hydrocarbon suppression (propane, butane, ethane, ethylene).[54] The introduction of 1% wt ceria on the support enhances ethanol selectivity compared to bare titania and produces a comparable product selectivity and CO conversion showed by $2Rh/TiO_2$[52] tested at higher pressure and temperature (20 bar and 435 K) (Figure 8 and 9).

The 2% wt. Rh catalysts supported on CeO_2-TiO_2 compared to 2% wt. Rh supported on ceria show lower ethanol and methanol selectivity but higher CO conversion (Figure 8 and 9). The superior ethanol selectivity achieved by $2Rh/CeO_2$ is at the expense of methane and C_2^+ hydrocarbon formation. Since the molecular weight of TiO_2 (79.8658 g/mol) is about half of CeO_2 (172.11 g/mol) and the mixed supports are composed of large quantities of TiO_2 (90-99% wt), a better comparison can be achieved when compared to 1%wt Rh on CeO_2. $1Rh/CeO_2$ has approximately the same ratio of Rh atoms per CeO_2 molecule as 2Rh/CeTi catalysts. $1Rh/CeO_2$ shows a lower CO conversion rate and higher ethanol selectivity due to methane suppression compared to 2Rh/CeTi catalysts. Methanol, C_2^+ hydrocarbons, and ethyl acetate are not formed when $1Rh/CeO_2$ was tested, while 2Rh/CeTi catalysts show the formation of these products.

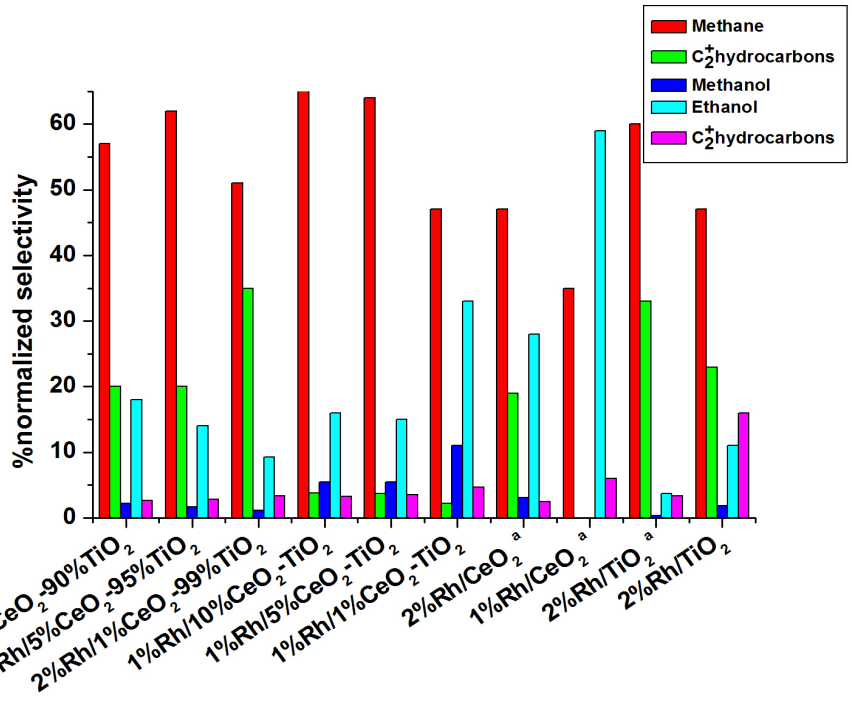

Figure 8. Effect of support on the product selectivity (%) on a series of unpromoted Rh catalysts. The reaction conditions and references can be found on Table 3. [(a)] Tests performed in our laboratory.

Comparing 2% wt. Rh supported on single TiO_2 and CeO_2 to the mixed oxides of ceria-titania, a synergetic effect between ceria and titania can be seen: the introduction of ceria increases ethanol selectivity but decreases CO conversion. Figure 7 shows that the the product distribution depends on the support.[73] In order to understand the shift on product distrubtion exhibited by 2Rh/CeTi catalyst, it is important to understand how how CO hydrogenation acts on Rh/CeO_2 and Rh/TiO_2. Ethanol formation on Rh/CeO_2 is produced by acetaldehyde hydrogenation where CeO_2 is not only support and can catalyze this step.[54] The decrease on CO hydrogenation activity of CeO_2 can be explained to the formation of highly stable acetate species on the surface of CeO_2 that are needed to be hydrogenated to form ethanol, or react with ethanol to form ethyl acetate. On the other hand, Rh/TiO_2 is more active towards CO hydrogenation due to the higher acidity of TiO_2 compared to

CeO_2.[53] The higher efficiency of TiO_2 is due to the transformation of CO into hydrocarbons than alcohols, the latter are preferred on more basic supports like CeO_2.

Previous studies suggest that ceria supported on titania is preferentially reduced (presence of Ce^{3+} cations) with Ce_2O_3 dimers stabilized on the planar TiO_2(110) surface.[64,62] The presence of reduced forms of ceria aid in the dispersion of the admetals (Rh and Fe in this work) and are known to form highly stable HCO_x species under CO exposure.[63, 74] The latter is the rls for ethanol formation on Rh-based catalysts.[25] TEM, TPR and XPS measurements performed on 1Rh/CeTi catalysts have suggested that electronic interactions between Rh and CeO_2 produce new active sites for CO hydrogenation at their interface.[61] It is highly likely that multiple catalytic sites are created on the 2Rh/CeTi catalysts as a result of interactions of Rh with TiO_2, CeO_2 and the interface of between CeO_2 and TiO_2.

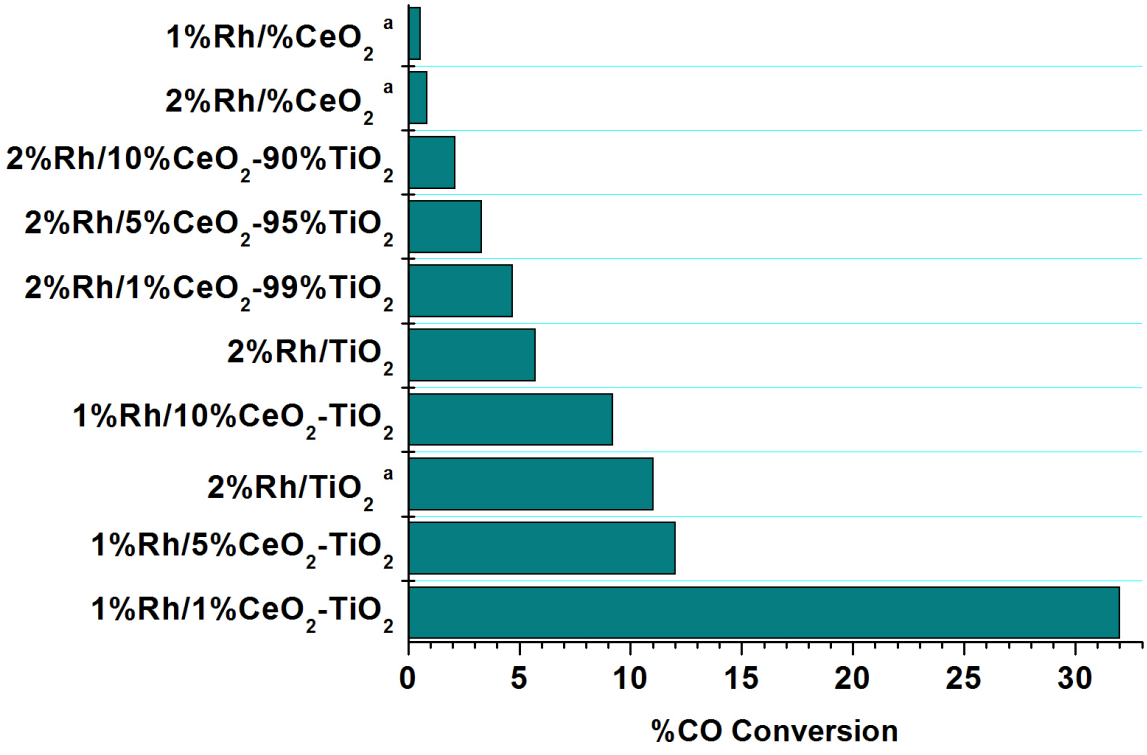

Figure 9. Effect of support on the CO conversion (%) on a series of unpromoted Rh-based catalysts. The reaction conditions are listed on Table 3.

Comparing the 2Rh/CeTi catalyst to a previous study using the same mixed-oxide composition but different reaction conditions and Rh loading[61], both catalysts series present different product selectivity distributions. Conversion of CO into products decreases with higher ceria loading for both Rh loadings (Figure 9). As for ethanol selectivity, this decreases with increasing ceria loading for 1Rh/CeTi, while for 2Rh/CeTi ethanol selectivity increases with ceria weight. The differences seen between 1Rh/CeTi and 2Rh/CeTi catalysts can be attributed to different Rh loading and higher reaction temperature and pressure.

The effect of Ce weight loading on titania has been tested on Pt/CeO_2-TiO_2 for the WGS.[75] Comparing Ce concentrations of 6% wt. and 15 % wt., the lowest loading showed the best WGS catalytic performance. As for methanol dehydration using a CuO/CeO_2-TiO_2 catalyst, a 9% wt. CeO_2 exhibited the highest conversion rate.[76] This Ce weight loading produces a higher dispersion of platinum and copper on the support.[75,76] A cerium surface layer on the titania particles is produced, which enhances the dispersion of the particles the active metal maximizing the number of active catalytic sites.[76] Therefore, the enhancement on ethanol selectivity when a 10% wt CeO_2 is introduced into titania can be attributed to its ability to act as a dispersing agent for Rh.

The introduction of ceria into titania as support for Rh in CO hydrogenation exhibits a synergistic behavior as compared to when the CeO_2 and TiO_2 are used as single supports. The mixed-oxide CeO_2-TiO_2 increases ethanol selectivity like pure CeO_2, but with higher CO conversion rates like TiO_2. Both ethanol selectivity and CO conversion of the 2% wt. Rh/CeO_2-TiO_2 catalyst is controlled by the amount of CeO_2 introduced into titania. Improved ethanol selectivity can be attributed to higher dispersion of Rh on the mixed oxide support, while the diminished CO conversion results from the formation of stable acetate species on the surface of CeO_2.

3.A.2. FE-PROMOTED, RH CATALYSTS

The use of iron as a promoter for supported 2% wt. Rh catalysts on the product selectivities for CO hydrogenation was studied for a range of promoter compositions. As it can be seen in Figure 9, 10 and 11 the selectivity for ethanol increases with iron weight loading achieving its maximum at a 8% wt Fe loading. The ethanol selectivity is comparable for FeRh supported on the 1CeTi, 5CeTi and 10CeTi mixed oxide supports when a 5% and an 8% wt Fe is used. For all of the three supports (Figures 10-12), the introduction of iron plays a major role since even at a low loading of 1% wt Fe the selectivity for ethanol is doubled and increases five-fold in the case of 1FeRh/1CeTi (Figure 12).

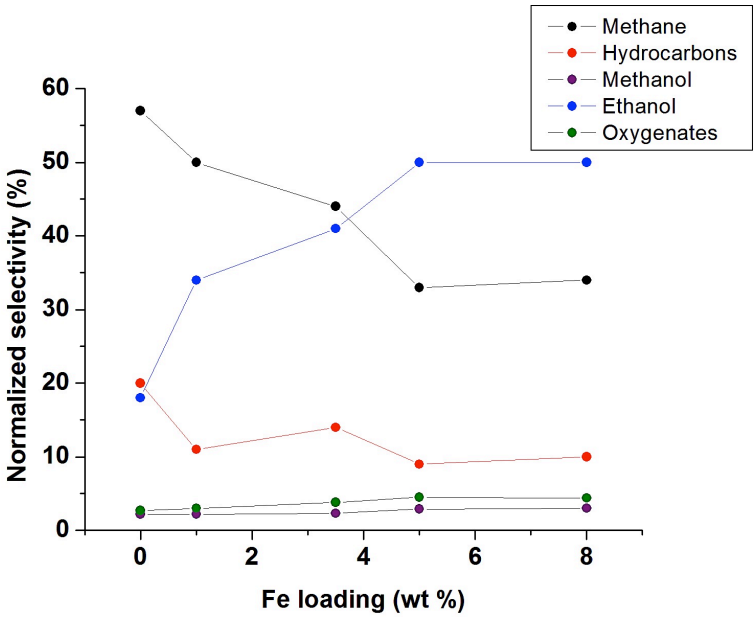

Figure 10. Effect of Fe loading on carbon selectivity (%) for Rh supported on 10%CeO2-90%TiO_2 (1bar, 513K, H_2:CO=2).

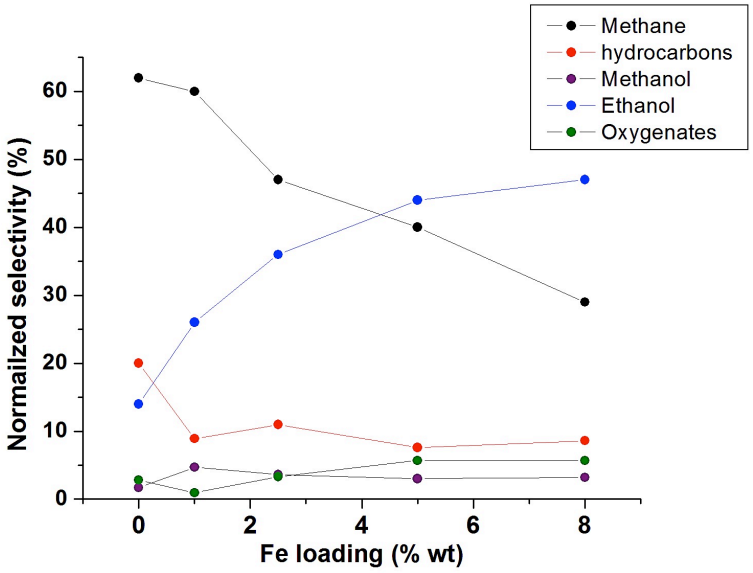

Figure 11. Effect of Fe loading on carbon selectivity (%) for Rh supported on 5%CeO$_2$-95%TiO$_2$ (1bar, 513K, H_2:CO=2).

The introduction of Fe decreases the formation of methane up to 50% compared to the unpromoted Rh-based catalysts supported on any of the three CeTi mixed oxide supports. In addition, methane suppression shows the same trends with Fe loading as ethanol selectivity but in the opposite direction. The production of hydrocarbons is also seen to drop initially with the introduction of Fe and then change slowly with the increase of Fe loading. The only C_2^+ hydrocarbons produced with the introduction of Fe are ethane and ethylene. Compared to their unpromoted counterparts, propane and butane production are absent with the addition of Fe on the 10CeTi, 5 CeTi and 1CeTi supports. Therefore, higher ethanol selectivity is mainly due to the decrease in methane formation and in minor proportion to C_2^+ hydrocarbon suppression.

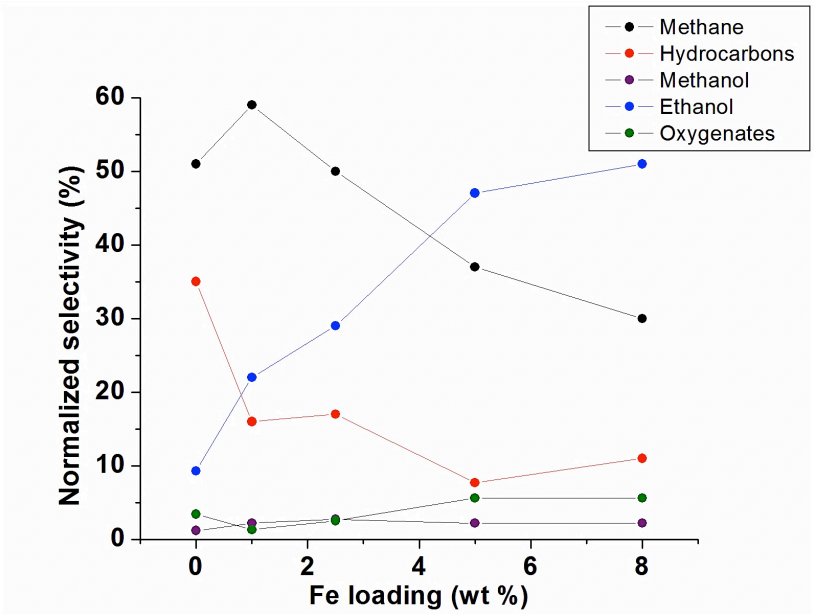

Figure 12. Effect of Fe loading on carbon selectivity (%) for Rh supported on 1%CeO$_2$-95%TiO$_2$ (1bar, 513K, H_2:CO=2).

The results from Fe-promotion are consistent with other studies (Figure 13) of CO hydrogenation performed over 2%Rh/TiO$_2$[52,69], 2%Rh/Al$_2$O$_3$[51], and 2%Rh/SiO$_2$[77]. All of these achieved high ethanol selectivities at similar Fe loadings due to methane suppression (Figure 14). This effect has been attributed to the close interaction between the metal and the promoter[51], and to suppression of H_2 chemisorption due to coverage of the active Rh surface.[52] On the other hand, lower Fe loadings (1.0 and 2.5%) on 2%Rh/CeO$_2$ (measurements performed in our laboratory) produce larger ethanol production (45 and 48%). Even though the product distribution seen with 2% wt Rh supported on the mixed oxides of CeO$_2$-TiO$_2$ is similar to 2%Rh/CeO$_2$, the effect of Fe loading on the product selectivities is more similar to 2%Rh/TiO$_2$. This shows that when Fe is added to the Rh supported on CeTi, both CeO$_2$ and TiO$_2$ work cooperatively but in a lesser extent to the unpromoted Rh/CeTi catalysts , and the main effect on ethanol selectivity is due to TiO$_2$ since is the major component on the support.

(a)

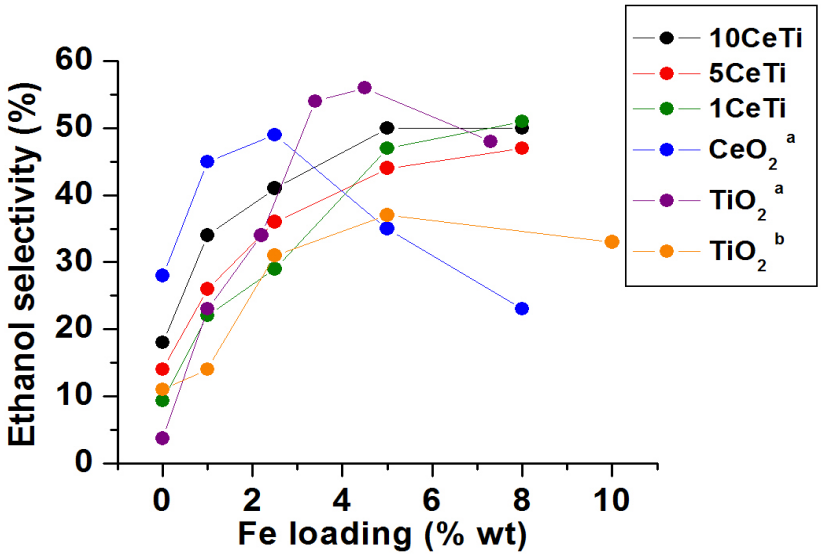

(b)

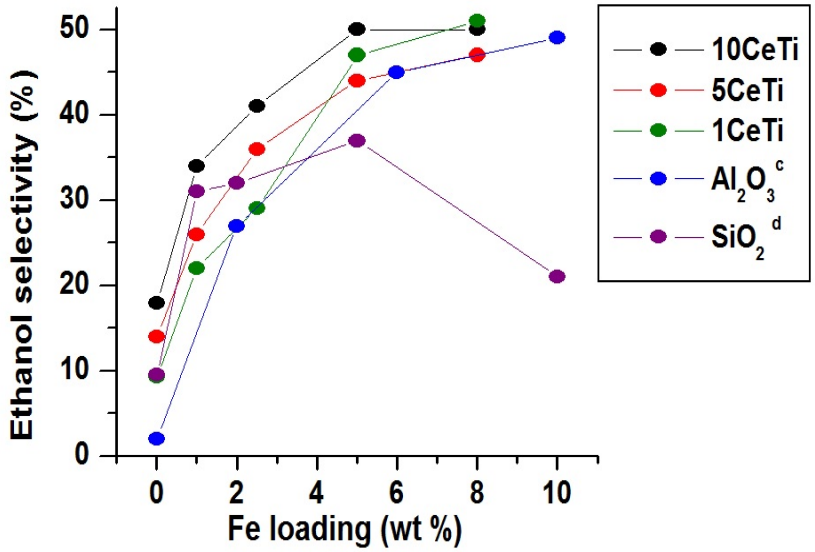

Figure 13. Comparison of ethanol selectivity versus Fe loading for Fe-promoted Rh catalysts supported on mixed CeO_2-TiO_2 supports, (a) single oxide supports of CeO_2 (2% wt Rh, reaction conditions of 1 bar, 513K, H2:CO=2:1) and TiO_2 (2% wt Rh, reaction conditions 10 bar, 430 K, H_2:CO=1)[51] and (b) single oxide supports of Al_2O_3 (2% wt Rh, reaction conditions of 20 bar, 543K, H_2:CO=1:1)[52] and SiO_2 (1% wt Rh, reaction conditions 20 bar, 523K, H_2:CO=2:1).[77]

(a)

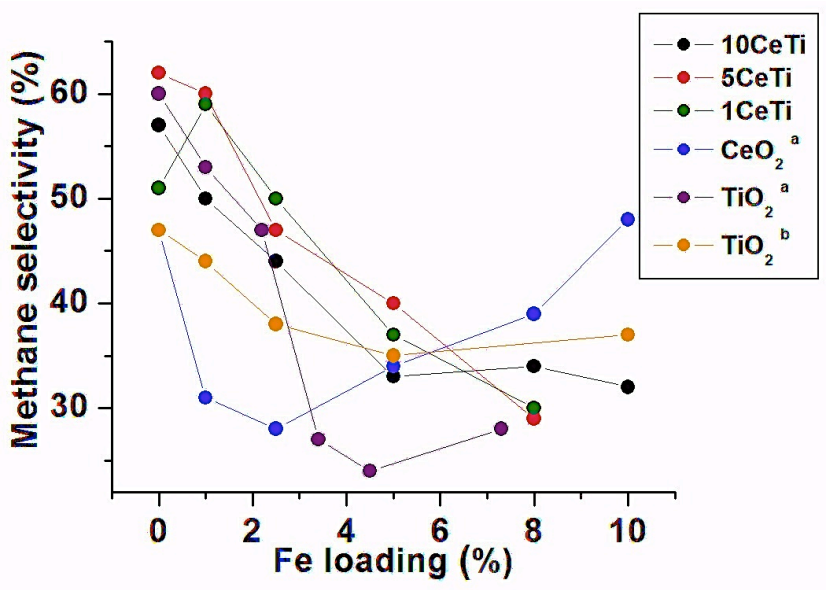

(b)

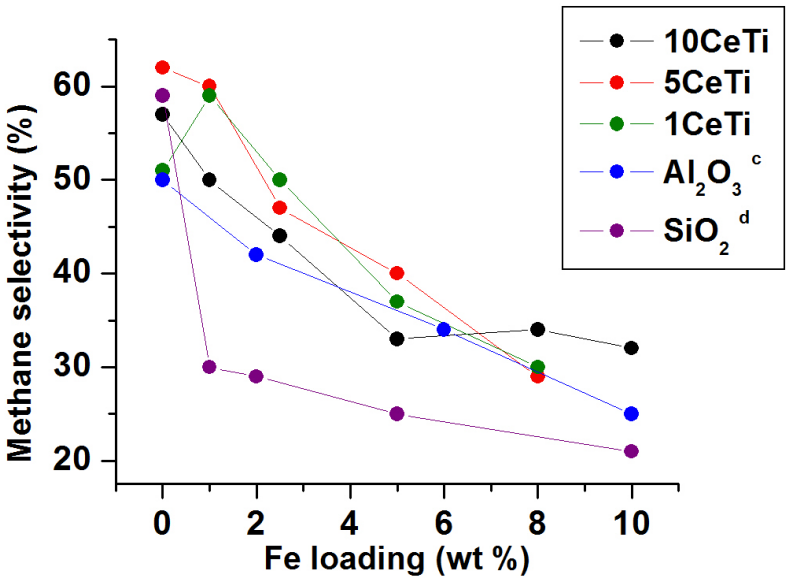

Figure 14. Comparison of methane selectivity versus Fe loading for Fe-promoted Rh catalysts supported on mixed CeO_2-TiO_2 supports, (a) single oxide supports of CeO_2 (2% wt Rh, reaction conditions of 1 bar, 513K, H_2:CO=2:1) and TiO_2 (2% wt Rh, reaction conditions 10 bar, 430 K, H_2:CO=1)[51] and (b) single oxide supports of Al_2O_3 (2% wt Rh, reaction conditions of 20 bar, 543K, H2:CO=1:1)[52] and SiO_2 (1% wt Rh, reaction conditions 20 bar, 523K, H_2:CO=2:1).[77]

(a)

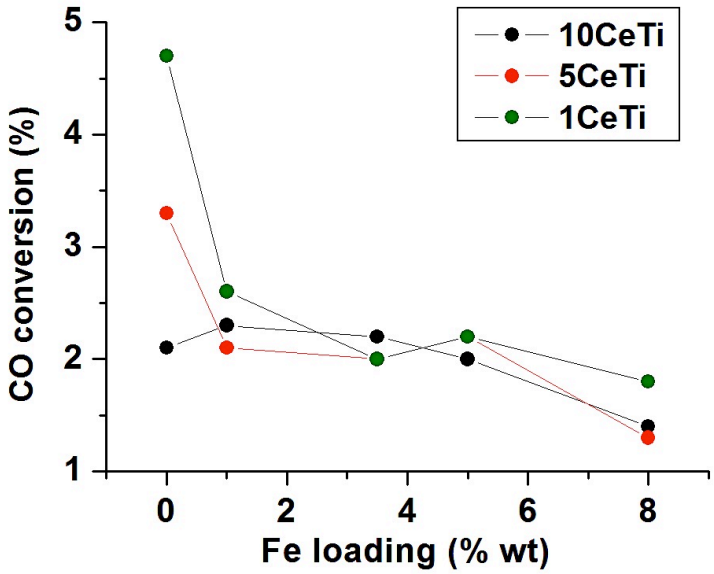

(b)

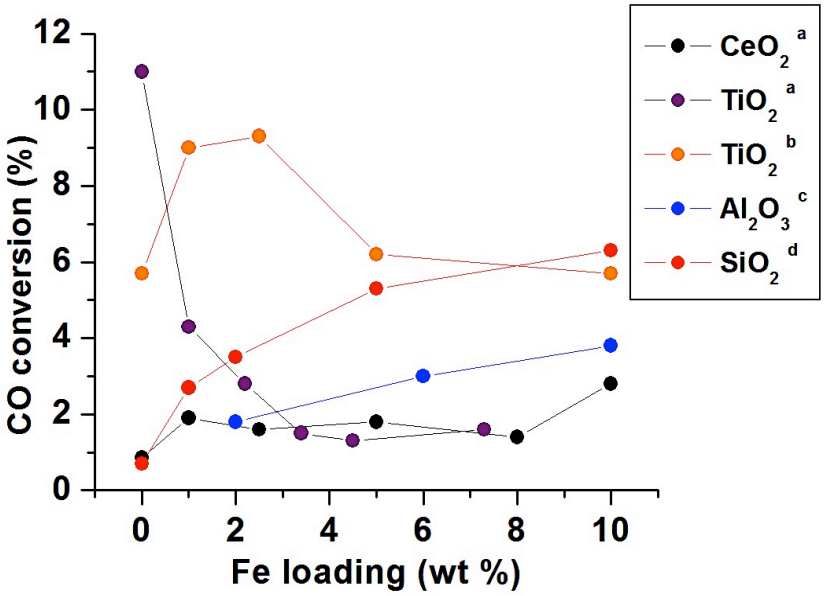

Figure 15. Comparison of CO conversion versus Fe loading for Fe-promoted Rh catalysts on different oxide supports: (a) mixed oxide supports of CeO_2-TiO_2 (b) single oxide supports of CeO_2 (2% wt Rh, reaction conditions of 1 bar, 513K, H_2:CO=2:1), TiO_2 (2% wt Rh, reaction conditions 10 bar, 430 K, H_2:CO=1),[51] $A_{l2}O_3$ (2% wt Rh, reaction conditions of 20 bar, 543K, H_2:CO=1:1)[52] and SiO_2 (1% wt Rh, reaction conditions 20 bar, 523K, H_2:CO=2:1).[77]

The addition of iron to the 2Rh/CeO_2-TiO_2 catalysts produces similar CO conversions despite the amount of ceria introduced to titania (Figure 15 (a)). Comparing to other supports like alumina and silica, the CeO_2-TiO_2 supports show lower CO conversions (Figure 15 (b)). Higher CO conversions for Fe-Rh alloys on SiO_2 and Al_2O_3 can be largely attributed to the significantly higher reaction pressures used in those studies.[51,77]

Therefore, regardless of the support used there is an enhancement on ethanol selectivity when iron is introduced due to methane suppression. Fe prefers to prefer to stay on the Rh surface[50] favoring the interaction with the adsorbates like CO improving ethanol production by increasing the energy barrier of methane formation and lowering the energy barrier for CO insertion . The decrease in CO conversion and shift in the product distributions when iron is added to the unpromoted Rh catalysts is indicative of the synergetic effect of the mixing of Rh and Fe. This has been attributed to alloy formation which produces modified active sites compared to Rh alone.[69] Ethanol selectivity reaches a maximum at a Fe loading of 5% wt for all the oxide supports studied here and reported in the literature (Figure 13). Consequently, it can be inferred that the active Fe-Rh phases present in all these catalysts is not dependent on the oxide support. By contrast, the support plays an important role in overall catalytic activity as can be seen in CO conversion rates (Figure 15). It is important to mention that larger CO conversion rates have been produced at higher temperatures and pressures compared to that used in this work which can boost the equilibrium concentration of products.[5]

2.A. CHARACTERIZATION BY IN-SITU XRD

2.A.1. CHARACTERIZATION OF BARE SUPPORT 10CeTi

The mixed oxide support that resulted in the highest ethanol selectivity was characterized by XRD using synchrotron radiation: 10CeTi. As it can be seen in Figure 16 and 17, the pure titania and ceria synthesized by this method yield single phase anatase and cerianite powders, respectively. On the other hand, Rietveld analysis identified and quantified three phases in the mixed 10CeTi oxide: anatase TiO_2, TiO_2(B), and cerianite. TiO_2(B) was firstly synthesized from $K_2Ti_4O_9$,[81] and has also been found in nature associated with anatase crystals yet there is no data of how common is in natural sources.[82] TiO_2(B) can be transformed into anatase at atmospheric pressure at temperatures above 550^oC or at room temperature at elevated pressures.[83] This transformation can be explained due to its common structural face centered-cubic unit cell. The differences between TiO_2 and anatase reside in their different space group (C2/m: TiO_2(B) and I41/amd:anatase), crystal system (monoclinic: TiO_2(B), tetragonal: anatase) and cell volume (35.3 $Å^3$: TiO_2(B) and 34.0 $Å^3$: anatase).[81,82,83] Comparing the diffraction patterns of the single supports to the mixed oxide support, the diffraction peaks due to cubic CeO_2 (Figure 17) and anatase TiO_2 (Figure 16) are broader and weaker than in the mixed oxide (Figure 18). This suggests lower crystallinity of the cubic CeO_2 and anatase TiO_2 phases, as well as a particle size decrease.

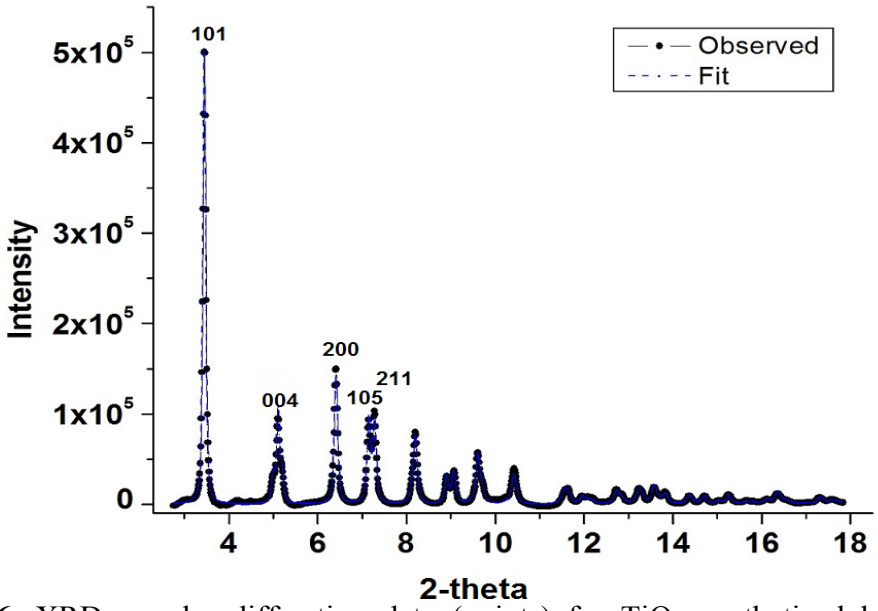

Figure 16. XRD powder diffraction data (points) for TiO_2 synthetized by the sol-gel technique and fitted to the anatase phase (line). The main peaks and their respective hkl Miller index planes are identified.

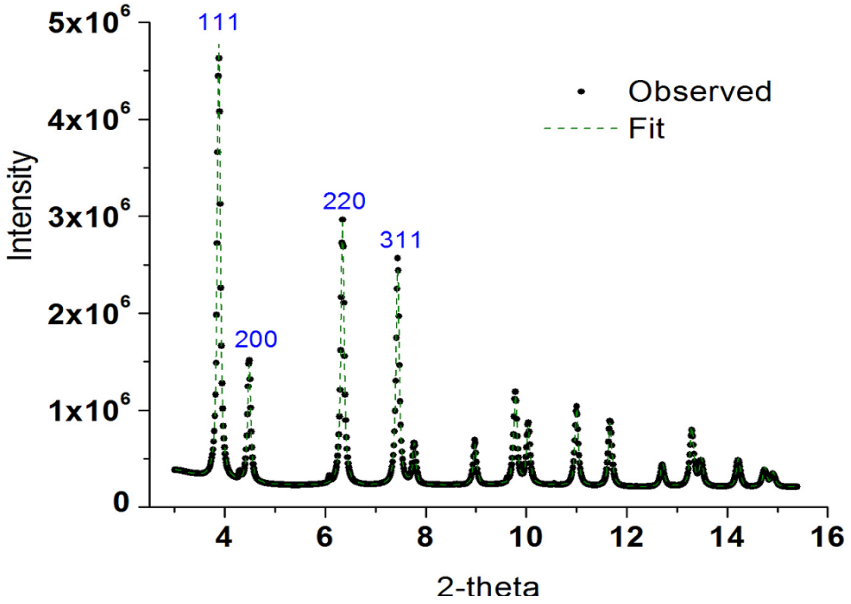

Figure 17. XRD powder diffraction data (points) for CeO_2 synthetized by the sol-gel technique and fitted to the cerianite phase (line). The main peaks and their respective hkl Miller index planes are identified.

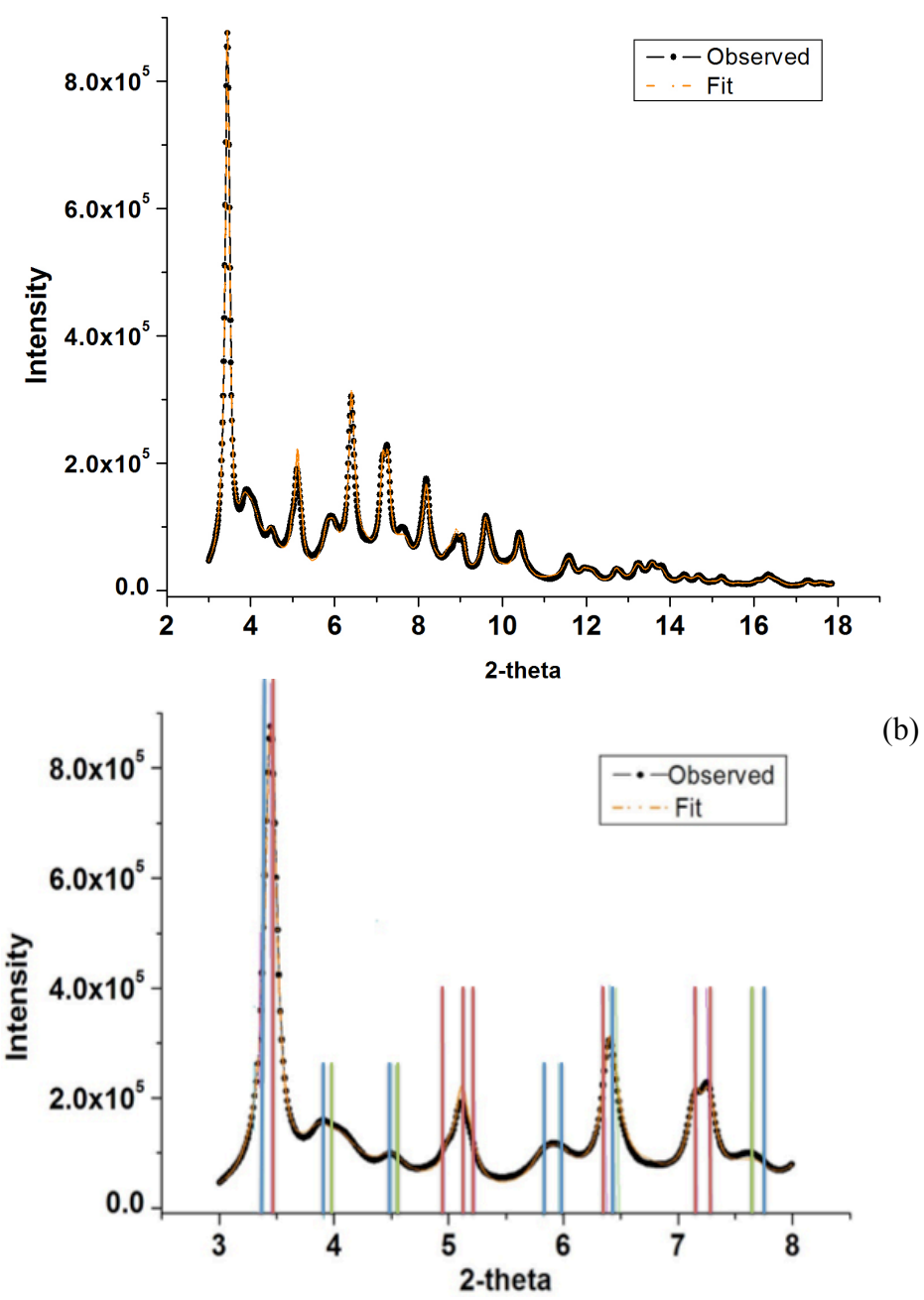

Figure 18. XRD pattern of the synthetized 10%CeO_2-90%TiO_2. (a) Fitting to three phases: anatse, TiO_2(B) and cerianite, (b) Main diffraction peaks of the phases present. Red: anatase, blue: TiO_2(B), and green: cerianite.

Figure 17 (a) shows the full XRD pattern of the synthetized 10%TiO_2-CeO_2 along with the fitting composed of three phases TiO_2(B), anatase, and cerianite. TiO_2(B)

diffraction peaks can be overlooked in some cases[83] where only laboratory XRD measurements have been perforemed.[79,64,59] The main reason could be due to the lower peak resolution and signal-to-noise ratio of laboratory XRD measurements compared to synchrotron XRD measurements. Furthermore, TiO_2(B)'s main diffraction peaks appear very close to the ones from cerianite and anatase (Figure 18 (a)). In order to see this more clearly, the main diffraction peaks and their respective reflective planes are indicated on Figure 18 (b) and listed in Table 4.

Table 4. Reflective planes of the phases present on 10%CeO_2-90%TiO_2 and their respective peak position.

Anatase		TiO_2(B)		Cerianite	
hkl	**2-theta(°)**	**hkl**	**2-theta (°)**	**hkl**	**2-theta (°)**
(101)	3.45	**(110)**	3.40	**(111)**	3.96
(103)	4.99	**(002)**	3.88	**(200)**	4.57
(004)	5.11	**(310)**	4.50	**(220)**	6.47
(112)	5.20	**(003)**	5.84	**(311)**	7.58
(200)	6.40	**(60-1)**	5.97		
(105)	7.15	**(020)**	6.46		
(211)	7.27	**(71-1)**	7.69		

The synthetized 10%CeO_2-90%TiO_2 is composed of anatase (48% wt ±3), TiO_2(B) (41% wt ±2) and in minor proportion, cerianite (11%wt. ±2). The slighltly higher content of CeO_2 compared to the nominal 10% wt added in the synthesis procedure needs to be further by ICP-OES measurements but the values found are in a good agreement with nomimal content weighed in the synthetic procedure. Previous studies performed on 10%CeO_2-90%TiO_2 have identified only two phases: anatase and cerianite, using nitric acid as pH regulator and hydrolysis agent.[84, 67, 66, 85] On the other hand, 10CeTi was synthetized using hydrochloric acid that produces chloride anions that can lead to poorly crystallized anatase phase.[86] The coexistence of TiO_2(B) and anatase can be explained due their similar fcc

structure,[83] and to the existence of a TiO_2(B) surface which may be stabilized by the presence of CeO_2. The latter effect has previously reported for a mixed oxide of SiO_2-TiO_2.[87]

Looking at the lattice parameters of anatase and TiO_2(B) in the mixed oxide, these are not significantly modified compared to pure anatase and to the reference for TiO_2(B).[82] Conversely, the unit cell parameters for cerianite are larger for pure ceria than in the mixed oxide, which has also been seen in previous studies under the same synthetic procedure[84, 67, 66, 85] In addition, the fitted lattice parameters do not indicate the presence of solid solutions in the mixed oxide. Overall, the synthesized CeO_2-TiO_2 mixed oxide is composed of titania mainly present in the form of anatase (48% wt.) and TiO_2(B) (41% wt), the latter attributed to the introduction of the of CeO_2 (11% wt.) which is supported on the titania matrix.

Table 5. Lattice parameters of CeO_2, TiO_2 and 10CeTi

		a	b	c
Anatase (TiO_2)	Literature	3.785		9.5133
	Single support	3.777 (±0.002)		9.476 (±0.004)
	10CeTi	3.789 (±0.001)		9.491(±0.004)
Cerianite (CeO_2)	Literature	5.411		
	Single support	5.402 (±0.001)		
	10CeTi	5.310 (±0.02)		
TiO_2(B)	10CeTi	12.20 (±0.02)	3.753 (±0.006)	6.564 (±0.02)
	Reference[82]	12.16	3.74	6.51

2.A.2. IN-SITU CHARACTERIZATION OF 2RH/10CETI

The unpromoted Rh based catalyst that showed the best ethanol selectivity was characterized as-synthesized, reduced, and under CO hydrogenation conditions. There was not a variation of the phases present under different reaction conditions compared to the bare 10CeTi. Rh phases could not be determined on the as-synthesized, reduced or under CO hydrogenation conditions for 2Rh/10CeTi. For the as-synthesized catalyst, rhodium (III) oxide could not be detected. The main two reflections of Rh_2O_3 (104) and (101)[88] located at 4.44^o and 4.72^o are overlapped by diffraction peaks from TiO_2(B) and cerianite. Similarly for the reduced sample or under CO hydrogenation conditions, no metallic Rh[89] could be detected despite the absence of overlapping peaks with its main reflection (104) located at 4.44^0.[90] This is indicative that Rh is highly dispersed on the support. The same ability of ceria to produce metal dispersion has been identified in previous studies of the mixed oxide CeO_2-TiO_2,[64,62,76,91] and has been correlated to increased catalytic activity. On the other hand, highly dispersed Rh particles have previously been reported by EXAFS studies of Rh supported on TiO_2 under reduction and CO hydrogenation conditions.[92,93,94] The overall picture to emerge from these results is that the decrease in the detectable ceria phase can be attributed to the formation of amorphous CeO_x species that also act as dispersing agents for Rh. The latter maximizes the number of Rh active sites for the formation of stable formyl species that translates into enhanced oxygenate formation when 10CeTi is used as support.

2.A.3. IN-SITU XRD CHARACTERIZATION OF 5FE2RH/10CEO$_2$-TIO$_2$

For understanding the role of Fe as promoter agent in ethanol production the evolution of its species, 3Fe/10CeTi was analyzed and compared to the sample that showed the best ethanol selectivity, i.e., 5Fe 2Rh/10CeTi. The 2-theta XRD patterns showing the Fe phases for 3Fe/10CeTi obtained by Rietveld analysis are presented in Figure 19. For the synthesized sample, the only FeO_x quantified was Fe_3O_4 (Table 6) by its main reflection plane (111) located at 4.82^o.[90] The amount of Fe_3O_4 (1.9%) is lower than the amount of Fe

introduced in the synthesis since other iron oxides (FeO and Fe_2O_3) can be present. FeO and Fe_2O_3 present reflection planes that are overlapped by the oxide components of the support. This could be accounted for the remaining Fe loading, which still needs to be confirmed by ICP-OES measurements. When reduced, a strong peak develops at 5.98^O corresponding to the Fe(110) reflection. Only a 0.3% wt Fe was quantified (compared to the 3% wt Fe added during the synthesis). This can be attributed to the presence of FeOx species that are highly dispersed or amorphous.[69] Under CO hydrogenation conditions the Fe (Table 7) is present only as Fe_3C as observed from the (110) plane at 5.82^o. The presence of iron carbides has been identified for CO hydrogenation and Fischer Tropsh synthesis (FTS) under reaction conditions in previous studies.[69,95]

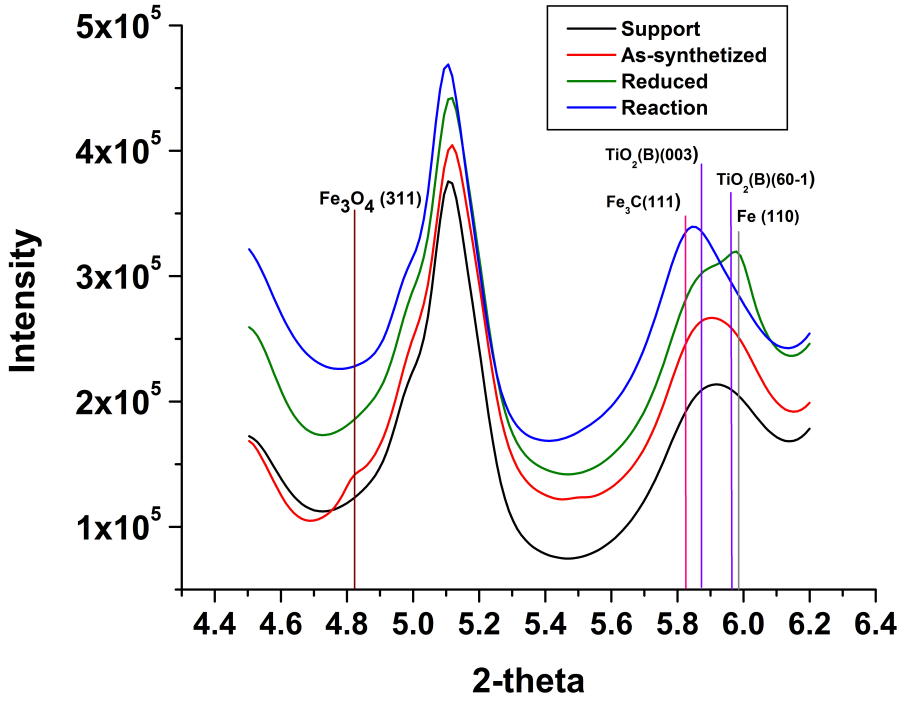

Figure 19. XRD curves for 3Fe/10CeTi for different treatments and under reaction conditions and compared to the bare support.

Figure 20 depicts the evolution of 5Fe2H/10CeTi across different reactions conditions and the identification of the main phases present. For the as-synthesized catalysts no Rh_2O_3 was observable whereas a very low amount of Fe_3O_4 (Table 7) was identified. The identification and quantification of Fe_3O_4 followed the same behavior seen on 3Fe/10CeTi. The reduced catalyst shows the presence of a Fe0.7Rh0.3 alloy evidenced by the diffraction peak centered at 5.84^0. The presence of this alloy has previously been identified for a similar loading of Fe and Rh supported on TiO_2.[69] The smaller content of Fe (Table 7) present as Fe0.7Rh0.3 alloy is likely due to the coexistence of other Fe phases like FeRh, FeO_x and metallic Fe[69] which could not be clearly identified due to overlap with the very broad peak from the oxide support. Under CO hydrogenation conditions, the appearance of Fe_3C is observed with an increase of Fe0.7Rh0.3 content (Table 7). The carburization of Fe is seen for both the 3Fe/10CeTi and 5Fe2Rh/10CeTi under reaction conditions. 3Fe/10CeTi was not active for ethanol production whereas 5Fe2Rh/10CeTi has high ethanol selectivity. These results indicate that the Fe0.7Rh0.3 alloy phases plays the main role for ethanol promotion on 5Fe2Rh/10CeTi while the presence of Fe_3C is seen as a spectator or deactivated phase so its effect on CO hydrogenation is not significant.[95]

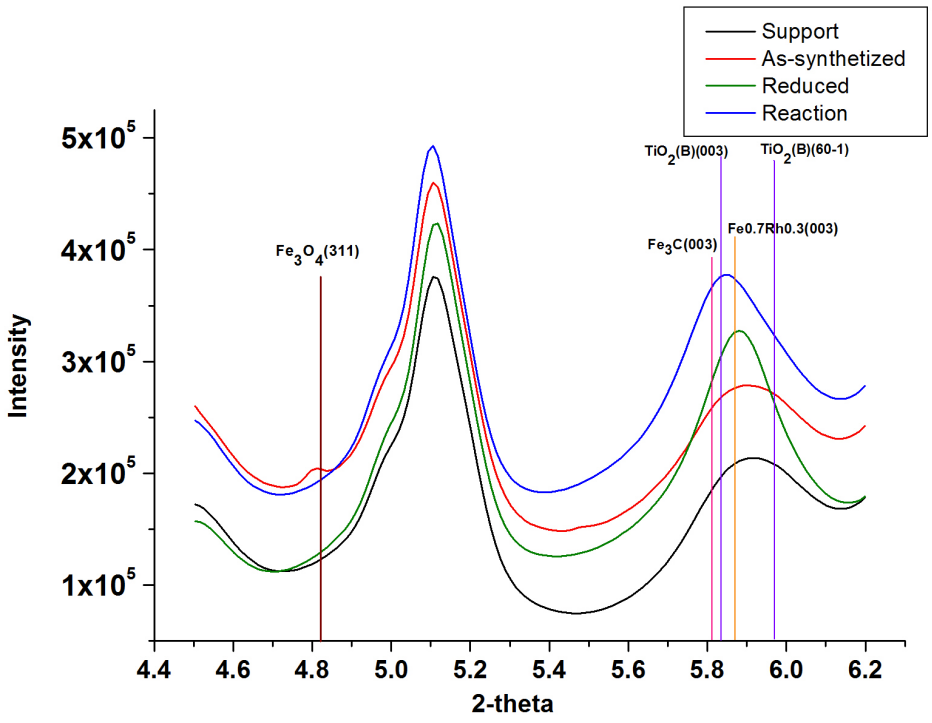

Figure 20. XRD curves for 5Fe2Rh/10CeTi for different treatments and under reaction conditions and compared to the bare support.

Table 6. Phase contents under different reactions conditions for 3Fe/10CeTi and 5Fe2Rh/10CeTi

Conditions	Phase	3Fe/10CeTi	5Fe2Rh/10CeTi
As-synthetized	Fe_3O_4	1.9% (±0.9%)	1.3% (±0.5%)
Reduced	Fe	0.3% (±0.2%)	-
	$Fe_{0.7}Rh_{0.3}$	-	1.2% (±0.3%)
CO hydrogenation	Fe_3C	3.9% (±3.0%)	1.5% (±0.2%)
	$Fe_{0.7}O_{0.3}$	-	2.8% (±0.3%)

CHAPTER 4

CONCLUSIONS

The modification of titania with ceria used as support for Rh-based nanocatalysts promotes ethanol selectivity. Ethanol production is enhanced with increasing ceria content in the CeO_2-TiO_2 mixed oxide support, reaching a maximum of 18% selectivity and the suppression of C_2^+ hydrocarbon formation for 10%CeO_2. The shift in product distributions and CO conversion rates of Rh/CeTi catalysts compared to Rh supported on the single TiO_2 or CeO_2 oxides are attributed to a synergetic effect between CeO_2 and TiO_2; it is also likely that Rh nanoparticles are supported on both the ceria and titania components in the mixed oxide. Furthermore, it can be explained by the formation of amorphous and mobile species of CeO_x that can act to improve Rh particle dispersion as very small nanaoparticles. The latter is thought to increase Rh catalytic sites for CO insertion and for the stabilization of HCO_x species that improve ethanol formation. The sol-gel synthesized bare 10CeTi mixed oxide is composed of (48% wt.), TiO_2(B) (41% wt) and cerianite (11% wt). The presence of TiO_2(B) is attributed to the introduction of CeO_2 into TiO_2. In-situ XRD analysis of the 2Rh/10CeTi showed no detectable Rh^0.When Fe is introduced as promoter, ethanol enhancement on the mixed oxide support is comparable to similar studies performed with other single oxide supports such as TiO_2, Al_2O_3 and SiO_2. Ethanol selectivity and methane suppression increases with Fe content, but the overall CO conversion or activity of the catalysts is also lowered. Rietveld refinement analysis of the XRD data for the 5Fe2Rh/10CeTi catalysts shows that Fe addition leads to the formation of a Fe-Rh alloy (Fe0.7Rh0.3). The presence of the Fe-Rh alloy has the largest impact for enhancing ethanol selectivity, which is attributed to a lowering of the CO insertion and increasing the methane formation energy barriers. Changes in oxide support have a much smaller effect on ethanol selectivity, but Fe-Rh supported on single oxide ceria and titania supports exhibit the highest catalytic performance to date. The mixed CeO_2-TiO_2 oxide supports exhibit catalytic performance for ethanol formation that is intermediate between the two separate components, but unfortunately the mixed oxide supports also show the lowest overall CO conversion. It is clear from these studies that the challenge for future work is to combine

the high ethanol selectivity of catalysts such as those studied in this work with much higher CO conversion (activity). Such improvements will be necessary to make CO/CO_2 hydrogenation for ethanol synthesis a more efficient and industrially viable process for producing simple liquid fuels.

BIBLIOGRAPHY

1 "2014 Key World Energy Statistics", (2014).

2 P. S. Nigam and A. Singh, "Production of liquid biofuels from renewable resources," Prog. Energy Combust. Sci. **37** (1), 52-68 (2011).

3 A. Demirbas, "Progress and recent trends in biofuels," Prog. Energy Combust. Sci. **33** (1), 1-18 (2007).

4 A. K. Agarwal, "Biofuels (alcohols and biodiesel) applications as fuels for internal combustion engines," Prog. Energy Combust. Sci. **33** (3), 233-271 (2007).

5 J. J. Spivey and A. Egbebi, "Heterogeneous catalytic synthesis of ethanol from biomass-derived syngas," Chem. Soc. Rev. **36** (9), 1514-1528 (2007).

6 V. Subramani and S. K. Gangwal, "A review of recent literature to search for an efficient catalytic process for the conversion of syngas to ethanol," Energy Fuels **22** (2), 814-839 (2008).

7 L. Gradisher, B. Dutcher, and M. Fan, "Catalytic hydrogen production from fossil fuels via the water gas shift reaction," Applied Energy **139**, 335-349 (2015).

8 Caitlin A. Callaghan, Worcester Polytechnic Institute, 2006.

9 Yixiong Yang, Michael G. White, and Ping Liu, "Theoretical Study of Methanol Synthesis from CO2 Hydrogenation on Metal-Doped Cu(111) Surfaces," The Journal of Physical Chemistry C **116** (1), 248-256 (2012).

10 Qian-Lin Tang, Qi-Jun Hong, and Zhi-Pan Liu, "CO2 fixation into methanol at Cu/ZrO2 interface from first principles kinetic Monte Carlo," Journal of Catalysis **263** (1), 114-122 (2009).

11 R. G. Herman, "Advances in catalytic synthesis and utilization of higher alcohols," Catal. Today **55** (3), 233-245 (2000).

12 William S. Epling, Gar B. Hoflund, and David M. Minahan, "Reaction and Surface Characterization Study of Higher Alcohol Synthesis Catalysts: VII. Cs- and Pd-Promoted 1:1 Zn/Cr Spinel," Journal of Catalysis **175** (2), 175-184 (1998).

13 John G. Nunan, Richard G. Herman, and Kamil Klier, "Higher alcohol and oxygenate synthesis over Cs/Cu/ZnO/M2O3 (M □ Al, Cr) catalysts," Journal of Catalysis **116** (1), 222-229 (1989).

14 Kazuhiko Takeuchi, Takehiko Matsukaki, Hironori Arakawa, and Yoshihiro Sugi, "Synthesis of ethanol from syngas over Co-Re-Sr/SiO2 Catalysts," Applied Catalysis **18** (2), 325-334 (1985).

15 M. Pijolat and V. Perrichon, "Synthesis of alcohols from CO and H2 on a Fe/A1203 catalyst at 8-30 bars pressure," Applied Catalysis **13** (2), 321-333 (1985).

16 Kazuhiko Takeuchi, Takehiko Matsuzaki, Taka-Aki Hanaoka, Hironori Arakawa, Yoshihiro Sugi, and Kemei Wei, "Alcohol synthesis from syngas over cobalt catalysts prepared from Co2(CO)8," Journal of Molecular Catalysis **55** (1), 361-370 (1989).

17 Xianguo Li, Lijuan Feng, Zhenyu Liu, Bing Zhong, Dady B. Dadyburjor, and Edwin L. Kugler, "Higher Alcohols from Synthesis Gas Using Carbon-Supported Doped Molybdenum-Based Catalysts," Ind. Eng. Chem. Res. **37** (10), 3853-3863 (1998).

18 Minglin Xiang, Debao Li, Wenhuai Li, Bing Zhong, and Yuhan Sun, "Potassium and nickel doped β-Mo2C catalysts for mixed alcohols synthesis via syngas," Catal. Commun. **8** (3), 513-518 (2007).
19 Minglin Xiang, Debao Li, Wenhuai Li, Bing Zhong, and Yuhan Sun, "Synthesis of higher alcohols from syngas over K/Co/β-Mo2C catalysts," Catal. Commun. **8** (3), 503-507 (2007).
20 R.R. Stevens, "Process for producing alcohols from synthesis gas", (Google Patents, 1989).
21 Jamshid Iranmahboob and DonaldO Hill, "Alcohol Synthesis from Syngas over K2CO3/CoS/MoS2 on Activated Carbon," Catalysis Letters **78** (1-4), 49-55 (2002).
22 Jamshid Iranmahboob, Hossein Toghiani, and Donald O. Hill, "Dispersion of alkali on the surface of Co-MoS2/clay catalyst: a comparison of K and Cs as a promoter for synthesis of alcohol," Applied Catalysis A: General **247** (2), 207-218 (2003).
23 Vivek Polshettiwar and Rajender S. Varma, "Green chemistry by nano-catalysis," Green Chem. **12** (5), 743-754 (2010).
24 B. R. Cuenya, "Synthesis and catalytic properties of metal nanoparticles: Size, shape, support, composition, and oxidation state effects," Thin Solid Films **518** (12), 3127-3150 (2010).
25 YongMan Choi and Ping Liu, "Mechanism of Ethanol Synthesis from Syngas on Rh(111)," Journal of the American Chemical Society **131** (36), 13054-13061 (2009).
26 M. Gupta, M. L. Smith, and J. J. Spivey, "Heterogeneous Catalytic Conversion of Dry Syngas to Ethanol and Higher Alcohols on Cu-Based Catalysts," ACS Catal. **1** (6), 641-656 (2011).
27 Kevin J. Smith and Robert B. Anderson, "The higher alcohol synthesis over promoted Cu/ZnO catalysts," The Canadian Journal of Chemical Engineering **61** (1), 40-45 (1983).
28 Xu Xiaoding, E. B. M. Doesburg, and J. J. F. Scholten, "Synthesis of higher alcohols from syngas - recently patented catalysts and tentative ideas on the mechanism," Catal. Today **2** (1), 125-170 (1987).
29 Pio Forzatti, Enrico Tronconi, and Italo Pasquon, "Higher Alcohol Synthesis," Catalysis Reviews **33** (1-2), 109-168 (1991).
30 Kai A. N. Verkerk, Bernd Jaeger, Caspar-Heinrich Finkeldei, and Wilhelm Keim, "Recent developments in isobutanol synthesis from synthesis gas," Applied Catalysis A: General **186** (1–2), 407-431 (1999).
31 David M. Minahan, William S. Epling, and Gar B. Hoflund, "Higher-alcohol synthesis reaction study V. Effect of excess ZnO on catalyst performance," Applied Catalysis A: General **166** (2), 375-385 (1998).
32 GarB Hoflund, WilliamS Epling, and DavidM Minahan, "An efficient catalyst for the production of isobutanol and methanol from syngas. XI. K‐ and Pd‐promoted Zn/Cr/Mn spinel (excess ZnO)," Catalysis Letters **62** (2-4), 169-173 (1999).
33 Edward M. Calverley and Kevin T. Smith, "The effects of carbon dioxide, methanol, and alkali promoter concentration on the higher alcohol synthesis over a Cu/ZnO/Cr2O3 catalyst," Journal of Catalysis **130** (2), 616-626 (1991).

34 Kamil Klier, Alessandra Beretta, Qun Sun, Owen C. Feeley, and Richard G. Herman, "Catalytic synthesis of methanol, higher alcohols and ethers," Catal. Today **36** (1), 3-14 (1997).
35 Martı Campos, amp, x, J. M. n, J. L. G. Fierro, A. Guerrero-Ruiz, R. G. Herman, and K. Klier, "Promoter Effect of Cesium on C–C Bond Formation during Alcohol Synthesis from CO/H2over Cu/ZnO/Cr2O3Catalysts," Journal of Catalysis **163** (2), 418-428 (1996).
36 D. Gall, E. J. Gibson, and C. C. Hall, "THE DISTRIBUTION OF ALCOHOLS IN THE PRODUCTS OF THE FISCHER-TROPSCH SYNTHESIS," Journal of Applied Chemistry **2** (7), 371-380 (1952).
37 Ahmad Razzaghi, Jean-Paul Hindermann, and Alain Kiennemanna, "Synthesis of c1 to c5 alcohols by co+h2 reaction on some modified iron-catalysts," Applied Catalysis **13** (1), 193-210 (1984).
38 Kaouru Fujimoto and Takamasa Oba, "Synthesis of C1-C7 alcohols from synthesis gas with supported cobalt catalysts," Applied Catalysis **13** (2), 289-293 (1985).
39 Masashi Inoue, Takanori Miyake, Yoshinobu Takegami, and Tomoyuki Inui, "Alcohol synthesis from syngas on ruthenium-based composite catalysts," Applied Catalysis **11** (1), 103-116 (1984).
40 S. Bordiga, E. Groppo, G. Agostini, J. A. van Bokhoven, and C. Lamberti, "Reactivity of Surface Species in Heterogeneous Catalysts Probed by In Situ X-ray Absorption Techniques," Chemical Reviews **113** (3), 1736-1850 (2013).
41 H. C. Woo, T. Y. Park, Y. G. Kim, In- S. Nam, J. S. Lee, and J. S. Chung, "Alkali-Promoted Mos2 Catalysts for Alcohol Synthesis: the Effect of Alkali Promotiom and Preparation Condition on Activity and Selectivity", in *Studies in Surface Science and Catalysis*, edited by F. Solymosi L. Guczi and TÉTÉNyi P (Elsevier, 1993), Vol. Volume 75, pp. 2749-2752.
42 Elm C. Alyea, Dasen He, and Jueh Wang, "Alcohol synthesis from syngas: I. Performance of alkali-promoted Ni-Mo(MOVS) catalysts," Applied Catalysis A: General **104** (1), 77-85 (1993).
43 Huijie Qi, Debao Li, Cheng Yang, Yugang Ma, Wenhuai Li, Yuhan Sun, and Bing Zhong, "Nickel and manganese co-modified K/MoS2 catalyst: high performance for higher alcohols synthesis from CO hydrogenation," Catal. Commun. **4** (7), 339-342 (2003).
44 V. R. Surisetty, A. K. Dalai, and J. Kozinski, "Alcohols as alternative fuels: An overview," Appl. Catal. A-Gen. **404** (1-2), 1-11 (2011).
45 Atsushi Takeuchi and James R. Katzer, "Ethanol formation mechanism from carbon monoxide + molecular hydrogen," The Journal of Physical Chemistry **86** (13), 2438-2441 (1982).
46 Masaru Ichikawa and Takakazu Fukushima, "Mechanism of syngas conversion into C2-oxygenates such as ethanol catalysed on a SiO2-supported Rh-Ti catalyst," Journal of the Chemical Society, Chemical Communications (6), 321-323 (1985).
47 Atsushi Takeuchi and James R. Katzer, "Mechanism of methanol formation," The Journal of Physical Chemistry **85** (8), 937-939 (1981).

48 E. Guglielminotti, E. Giamello, F. Pinna, G. Strukul, S. Martinengo, and L. Zanderighi, "Elementary Steps in CO Hydrogenation on Rh Catalysts Supported on ZrO2 and Mo/ZrO2," Journal of Catalysis **146** (2), 422-436 (1994).
49 Andreas Kohl, Christian Linsmeier, Edmund Taglauer, and Helmut Knozinger, "Influence of support and promotor on the catalytic activity of Rh/VOx/SiO2 model catalysts," Physical Chemistry Chemical Physics **3** (21), 4639-4643 (2001).
50 L. Yang and P. Liu, "Ethanol Synthesis from Syngas on Transition Metal-Doped Rh(111) Surfaces: A Density Functional Kinetic Monte Carlo Study," Top. Catal. **57** (1-4), 125-134 (2014).
51 R. Burch and M. J. Hayes, "The preparation and characterisation of Fe-promoted Al2O3-supported Rh catalysts for the selective production of ethanol from syngas," Journal of Catalysis **165** (2), 249-261 (1997).
52 M. A. Haider, M. R. Gogate, and R. J. Davis, "Fe-promotion of supported Rh catalysts for direct conversion of syngas to ethanol," Journal of Catalysis **261** (1), 9-16 (2009).
53 James R. Katzer, Arthur W. Sleight, Patricio Gajardo, John B. Michel, Edward F. Gleason, and Scott McMillan, "The role of the support in CO hydrogenation selectivity of supported rhodium," Faraday Discussions of the Chemical Society **72** (0), 121-133 (1981).
54 Y. Q. Wang, J. Li, and W. L. Mi, "Probing study of Rh catalysts on different supports in CO hydrogenation," React. Kinet. Catal. Lett. **76** (1), 141-150 (2002).
55 S. S. C. Chuang, R. W. Stevens, and R. Khatri, "Mechanism of C2+ oxygenate synthesis on Rh catalysts," Top. Catal. **32** (3-4), 225-232 (2005).
56 L. P. Han, D. S. Mao, J. Yu, Q. S. Guo, and G. Z. Lu, "Synthesis of C-2-oxygenates from syngas over Rh-based catalyst supported on SiO2, TiO2 and SiO2-TiO2 mixed oxide," Catal. Commun. **23**, 20-24 (2012).
57 L. P. Han, D. S. Mao, J. Yu, Q. S. Guo, and G. Z. Lu, "C-2-oxygenates synthesis through CO hydrogenation on SiO2-ZrO2 supported Rh-based catalyst: The effect of support," Appl. Catal. A-Gen. **454**, 81-87 (2013).
58 J. B. Park, J. Graciani, J. Evans, D. Stacchiola, S. G. Ma, P. Liu, A. Nambu, J. F. Sanz, J. Hrbek, and J. A. Rodriguez, "High catalytic activity of Au/CeOx/TiO2(110) controlled by the nature of the mixed-metal oxide at the nanometer level," Proc. Natl. Acad. Sci. U. S. A. **106** (13), 4975-4980 (2009).
59 J. A. Rodriguez, P. Liu, J. Hrbek, J. Evans, and M. Perez, "Water gas shift reaction on Cu and Au nanoparticles supported on CeO2(111) and ZnO(000(1)over-bar): Intrinsic activity and importance of support interactions," Angew. Chem.-Int. Edit. **46** (8), 1329-1332 (2007).
60 Junji Nakamura, Joseph M. Campbell, and Charles T. Campbell, "Kinetics and mechanism of the water-gas shift reaction catalysed by the clean and Cs-promoted Cu(110) surface: a comparison with Cu(111)," Journal of the Chemical Society, Faraday Transactions **86** (15), 2725-2734 (1990).
61 Changming Li, Junmin Liu, Wa Gao, Yufei Zhao, and Min Wei, "Ce-Promoted Rh/TiO2 Heterogeneous Catalysts Towards Ethanol Production from Syngas," Catalysis Letters **143** (11), 1247-1254 (2013).

62 J. Graciani, J. J. Plata, J. F. Sanz, P. Liu, and J. A. Rodriguez, "A theoretical insight into the catalytic effect of a mixed-metal oxide at the nanometer level: The case of the highly active metal/CeOx/TiO2(110) catalysts," Journal of Chemical Physics **132** (10), 8 (2010).
63 J. A. Rodriguez and D. Stacchiola, "Catalysis and the nature of mixed-metal oxides at the nanometer level: special properties of MOx/TiO2(110) {M= V, W, Ce} surfaces," Physical Chemistry Chemical Physics **12** (33), 9557-9565 (2010).
64 J. B. Park, J. Graciani, J. Evans, D. Stacchiola, S. D. Senanayake, L. Barrio, P. Liu, J. F. Sanz, J. Hrbek, and J. A. Rodriguez, "Gold, Copper, and Platinum Nanoparticles Dispersed on CeOx/TiO2(110) Surfaces: High Water-Gas Shift Activity and the Nature of the Mixed-Metal Oxide at the Nanometer Level," Journal of the American Chemical Society **132** (1), 356-363 (2010).
65 C. S. Lim, J. H. Ryu, D. H. Kim, S. Y. Cho, and W. C. Oh, "Reaction morphology and the effect of pH on the preparation of TiO2 nanoparticles by a sol-gel method," J. Ceram. Process. Res. **11** (6), 736-741 (2010).
66 Jun Fang, Xinzhen Bi, Dejun Si, Zhiquan Jiang, and Weixin Huang, "Spectroscopic studies of interfacial structures of CeO2-TiO2 mixed oxides," Applied Surface Science **253** (22), 8952-8961 (2007).
67 C. Gionco, M. C. Paganini, S. Agnoli, A. E. Reeder, and E. Giamello, "Structural and spectroscopic characterization of CeO2-TiO2 mixed oxides," J. Mater. Chem. A **1** (36), 10918-10926 (2013).
68 P. J. Chupas, K. W. Chapman, C. Kurtz, J. C. Hanson, P. L. Lee, and C. P. Grey, "A versatile sample-environment cell for non-ambient X-ray scattering experiments," Journal of Applied Crystallography **41**, 822-824 (2008).
69 Robert M. Palomino, Joseph W. Magee, Jordi Llorca, Sanjaya D. Senanayake, and Michael G. White, "The effect of Fe–Rh alloying on CO hydrogenation to C2+ oxygenates," Journal of Catalysis **329** (0), 87-94 (2015).
70 A. P. Hammersley, S. O. Svensson, M. Hanfland, A. N. Fitch, and D. Hausermann, "Two-dimensional detector software: From real detector to idealised image or two-theta scan," High Pressure Research **14** (4-6), 235-248 (1996).
71 Brian Toby, "EXPGUI, a graphical user interface for GSAS," Journal of Applied Crystallography **34** (2), 210-213 (2001).
72 A.C. Larson and R.B. Von Dreele, 200.
73 F. Solymosi, I. Tombacz, and M. Kocsis, "HYDROGENATION OF CO ON SUPPORTED RH CATALYSTS," Journal of Catalysis **75** (1), 78-93 (1982).
74 Aaron C. Johnston-Peck, Sanjaya D. Senanayake, José J. Plata, Shankhamala Kundu, Wenqian Xu, Laura Barrio, Jesús Graciani, Javier Fdez Sanz, Rufino M. Navarro, José L. G. Fierro, Eric A. Stach, and José A. Rodriguez, "Nature of the Mixed-Oxide Interface in Ceria–Titania Catalysts: Clusters, Chains, and Nanoparticles," The Journal of Physical Chemistry C **117** (28), 14463-14471 (2013).
75 L. Barrio, G. Zhou, I. D. Gonzalez, M. Estrella, J. Hanson, J. A. Rodriguez, R. M. Navarro, and J. L. G. Fierro, "In situ characterization of Pt catalysts supported on ceria modified TiO2 for the WGS reaction: influence of ceria loading," Physical Chemistry Chemical Physics **14** (7), 2192-2202 (2012).

76 M. S. P. Francisco, V. R. Mastelaro, P. A. P. Nascente, and A. O. Florentino, "Activity and characterization by XPS, HR-TEM, Raman spectroscopy, and BET surface area of CuO/CeO2-TiO2 catalysts," J. Phys. Chem. B **105** (43), 10515-10522 (2001).
77 J. J. Wang, Q. H. Zhang, and Y. Wang, "Rh-catalyzed syngas conversion to ethanol: Studies on the promoting effect of FeOx," Catal. Today **171** (1), 257-265 (2011).
78 Qing-Zhi Yan, Xin-Tai Su, Zhen-Ying Huang, and Chang-Chun Ge, "Sol–gel auto-igniting synthesis and structural property of cerium-doped titanium dioxide nanosized powders," J. European Ceram. Soc. **26** (6), 915-921 (2006).
79 Jun Lin and Jimmy C. Yu, "An investigation on photocatalytic activities of mixed TiO2-rare earth oxides for the oxidation of acetone in air," Journal of Photochemistry and Photobiology A: Chemistry **116** (1), 63-67 (1998).
80 An-Wu Xu, Yuan Gao, and Han-Qin Liu, "The Preparation, Characterization, and their Photocatalytic Activities of Rare-Earth-Doped TiO2 Nanoparticles," J. Catal. **207** (2), 151-157 (2002).
81 R. Marchand, L. Brohan, and M. Tournoux, "TIO2(B) A NEW FORM OF TITANIUM-DIOXIDE AND THE POTASSIUM OCTATITANATE K2TI8O17," Materials Research Bulletin **15** (8), 1129-1133 (1980).
82 J. F. Banfield, D. R. Veblen, and D. J. Smith, "THE IDENTIFICATION OF NATURALLY-OCCURRING TIO2 (B) BY STRUCTURE DETERMINATION USING HIGH-RESOLUTION ELECTRON-MICROSCOPY, IMAGE SIMULATION, AND DISTANCE-LEAST-SQUARES REFINEMENT," American Mineralogist **76** (3-4), 343-353 (1991).
83 L. Brohan, A. Verbaere, M. Tournoux, and G. Demazeau, "THE TRANSFORMATION TIO2(B)- ANATASE," Materials Research Bulletin **17** (3), 355-361 (1982).
84 J. Fang, H. Bao, B. He, F. Wang, D. Si, Z. Jiang, Z. Pan, S. Wei, and W. Huang, "Interfacial and surface structures of CeO2-TiO2 mixed oxides," Journal of Physical Chemistry C **111** (51), 19078-19085 (2007).
85 T. Lopez, F. Rojas, R. Alexander-Katz, F. Galindo, A. Balankin, and A. Buljan, "Porosity, structural and fractal study of sol-gel TiO2-CeO2 mixed oxides," J. Solid State Chem. **177** (6), 1873-1885 (2004).
86 Damien Dambournet, Ilias Belharouak, and Khalil Amine, "Tailored Preparation Methods of TiO2 Anatase, Rutile, Brookite: Mechanism of Formation and Electrochemical Properties," Chemistry of Materials **22** (3), 1173-1179 (2010).
87 Toshihiro Kogure, Taku Umezawa, Yoshinori Kotani, Atsunori Matsuda, Masahiro Tatsumisago, and Tsutomu Minami, "Formation of TiO2(B) Nanocrystallites in Sol-Gel-Derived SiO2-TiO2 Film," J. Am. Ceram. Soc. **82** (11), 3248-3250 (1999).
88 J. M. D. Coey, "The crystal structure of Rh2O3," Acta Crystallographica Section B **26** (11), 1876-1877 (1970).
89 M. R. Gogate and R. J. Davis, "X-ray Absorption Spectroscopy of an Fe-Promoted Rh/TiO2 Catalyst for Synthesis of Ethanol from Synthesis Gas," Chemcatchem **1** (2), 295-303 (2009).
90 Luo Huey-Lin and Pol Duwez, "Solid Solutions of rhodium with copper and nickel," Journal of the Less Common Metals **6** (3), 248-249 (1964).
91 A. Cervantes, G. Del Angel, G. Torres, G. Lafaye, J. Barbier Jr, J. N. Beltramini, J. G. Cabañas-Moreno, and A. Espinosa de los Monteros, "Degradation of methyl tert-

butyl ether by catalytic wet air oxidation over Rh/TiO2–CeO2 catalysts," Catal. Today **212** (0), 2-9 (2013).

92 D. C. Koningsberger, J. H. A. Martens, R. Prins, D. R. Short, and D. E. Sayers, "The structure of a rhodium/titania catalyst in the strong metal-support interaction state as determined by EXAFS," The Journal of Physical Chemistry **90** (14), 3047-3050 (1986).

93 Stanley Sakellson, Martin McMillan, and Gary L. Haller, "EXAFS evidence for direct metal-metal bonding in reduced rhodium/titania catalysts," The Journal of Physical Chemistry **90** (9), 1733-1736 (1986).

94 J. H. A. Martens, R. Prins, H. Zandbergen, and D. C. Koningsberger, "Structure of rhodium/titania in the normal and the SMSI state as determined by extended x-ray absorption fine structure and high-resolution transmission electron microscopy," The Journal of Physical Chemistry **92** (7), 1903-1916 (1988).

95 Emiel de Smit, Andrew M. Beale, Sergey Nikitenko, and Bert M. Weckhuysen, "Local and long range order in promoted iron-based Fischer–Tropsch catalysts: A combined in situ X-ray absorption spectroscopy/wide angle X-ray scattering study," Journal of Catalysis **262** (2), 244-256 (2009).